

Topological magnon in exchange frustration driven incommensurate spin spiral of a kagome lattice YMn_6Sn_6

Banasree Sadhukhan,^{1,2} Anders Bergman,³ Patrik Thunström,³
Manuel Pereiro Lopez,³ Olle Eriksson,³ and Anna Delin^{2,4,5}

¹*Department of Physics and Nanotechnology, SRM Institute of Science and Technology, Kattankulathur, 603203, Chennai, Tamil Nadu, India**

²*Department of Applied Physics, School of Engineering Sciences,*

KTH Royal Institute of Technology, AlbaNova University Center, SE-10691 Stockholm, Sweden†

³*Department of Physics and Astronomy, Uppsala University, Box 516, SE-75120 Uppsala, Sweden*

⁴*Swedish e-Science Research Center (SeRC), KTH Royal Institute of Technology, SE-10044 Stockholm, Sweden*

⁵*Wallenberg Initiative Materials Science for Sustainability (WISE), KTH Royal Institute of Technology, SE-10044 Stockholm, Sweden*

YMn_6Sn_6 consists of two types of Mn-based kagome planes stacked along c -axis having a complex magnetic interactions. We report a spin reconstruction in YMn_6Sn_6 from ferromagnet (FM) into a combination of two incommensurate spin spirals (SSs) originating from two different type of Mn kagome planes driven by frustrated magnetic exchanges along the c -axis with inclusion of Hubbard U . The pitch angle and wave vector of the incommensurate SSs are $\sim 89.3^\circ$ and $\sim (0\ 0\ 0.248)$ respectively which are in excellent agreement with experiment. We employed an effective model Hamiltonian constructed out of exchange interactions to capture experimentally observed non-equivalent nature of the two incommensurate SSs which also explain FM-SS crossover due to antiferromagnetic spin exchange with correlation. We further report the existence of topological magnon with spin-orbit coupling in incommensurate SS phase of YMn_6Sn_6 by calculating the topological invariants and Berry curvature profile. The location of Dirac magnon in energy landscape at 73 meV matches with another experimental report. We demonstrate the accuracy of our results by highlighting experimental features in YMn_6Sn_6 .

Introduction : Magnetic kagome crystal, consisting of corner-sharing triangles, is an intriguing class of materials in condensed-matter physics because of having Chern gapped topological fermions, electronic flat bands, topological magnon, non-trivial Hall effect and non-trivial topology [16–23]. The co-existence of geometric frustration and strong electron-electron correlations makes kagome-lattice based systems an ideal system to study the interplay between magnetism and topology for next-generation spintronics [18]. Flat bands, with the quenching kinetic energy, appear in kagome magnets due to lattice geometry and hosts superconductivity [24].

Magnetic interactions in frustrated kagome materials are of great complexity and result in complicated non-collinear spin texture due to a delicate interplay between the symmetric Heisenberg exchange and asymmetric Dzyaloshinskii–Moriya interaction (DMI) which generates the spin canting. Recently, the Mn-based kagome magnets have attracted great attention stimulating vast investigations in the field of kagome materials. Mn_3X ($\text{X} = \text{Rh}, \text{Ir}, \text{Pt}, \text{Ga}, \text{Ge}, \text{Sn}$) consisting of layered kagome planes have a noncollinear antiferromagnetic (AFM) spin texture [25–28]. SOC induces a virtual tilting of the magnetic moments and chiral spin texture induces spin currents in the absence of an external magnetic field [28].

RMn_6Sn_6 is a sibling of Mn-based kagome family ($\text{R}=\text{rare earth element}$) where the R elements play an

important role in predicting the magnetic ground state. The spin moments of the localized rare-earth R-4f and itinerant transition metal Mn-3d orbitals are inclined antiparallel [29, 30] in heavy rare earth kagome systems, which leads to a ferrimagnetic ground state in $(\text{Gd}, \text{Tb}, \text{Dy}, \text{Ho}, \text{Er})\text{Mn}_6\text{Sn}_6$ compounds [31–33]. The magnetic coupling between the light R and Mn moment is parallel in $(\text{Nd}, \text{Sm})\text{Mn}_6\text{Sn}_6$ leading to a collinear FM ordering above room temperature [34]. Whereas, the isostructural $(\text{Sc}, \text{Y}, \text{Lu})\text{Mn}_6\text{Sn}_6$ with nonmagnetic R atoms shows a spin spiral (SS) ordering of Mn moment [34–40]. Therefore, exploring the real space spin texture in its ground state and their relationship with kagome lattice geometry merit further study in RMn_6Sn_6 family, especially when R is a non-magnetic.

YMn_6Sn_6 has a commensurate collinear structure above the room temperature which switches to a incommensurate phase upon cooling [39]. The incommensurate phase is very much sensitive to temperature and magnetic field [37]. However, YMn_6Sn_6 has been a subject of many recent experimental studies [35–40]. The intrinsic anomalous Hall effect is stemming from the Berry curvature field in Mn-based distorted kagome lattice [40]. Therefore, the relation between the topological electronic properties and complex magnetic behaviour in YMn_6Sn_6 has motivated wide interest in strongly correlated physics and makes a proliferate field to investigate the interplay between electron and spin.

The kagome magnets are candidates for quantum materials, but the distorted kagome magnets were rarely studied. Unlike other members of the kagome magnet

* banasres@srmist.edu.in

† banasree@kth.se

family, YMn_6Sn_6 consists of two types of segregated Mn kagome planes. Our spin dynamics simulation reports the magnetic ground state as a combination of two incommensurate SSs originating from two different sub-lattices of Mn atoms which is enforced due to exchange frustration along c -axis. We capture the ferromagnetic (FM) - SS crossover with AFM spin exchange in YMn_6Sn_6 . We employed an effective model Hamiltonian to understand the crossover physics of two non-equivalent and the incommensurate SSs microscopically. Dirac crossings appear in the magnon bands of YMn_6Sn_6 which open topological gap with inclusion of DMI. Our study is further collaborated by finding the Chern numbers and Berry curvature which confirm the existence of topological magnon in incommensurate SS phase of YMn_6Sn_6 .

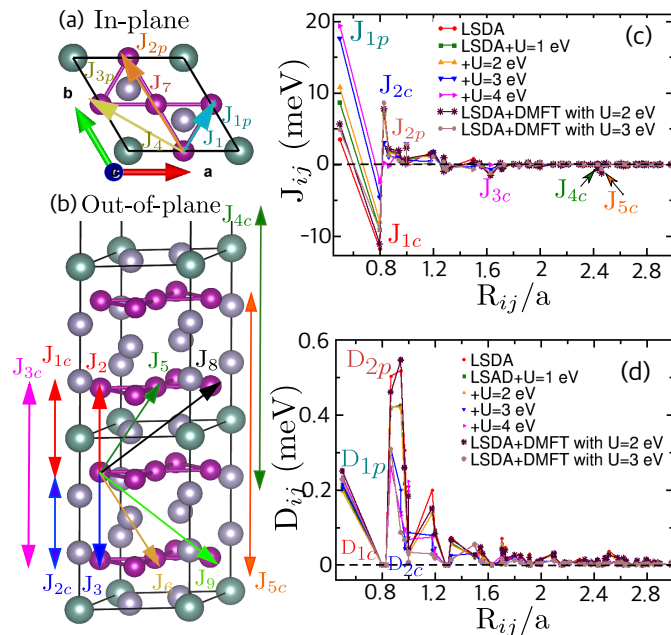


FIG. 1. (a)-(b) Magnetic exchange interactions for nearest neighbour (NN) mapping in YMn_6Sn_6 . The atoms in purple, green and gray colours represent Mn, Y, Sn atoms respectively. (c) Isotropic part of Heisenberg interactions J_{ij} 's and (d) anti-symmetric Dzyaloshinskii-Moriya interactions D_{ij} 's in YMn_6Sn_6 . Here we used the convention of positive (negative) J_{ij} 's as FM (AFM) and the subscript c (p) for c -axis (ab -plane) magnetic interactions throughout the text.

Complex magnetic interactions : YMn_6Sn_6 consists of two inequivalent Mn based kagome planes stacking along the c -axis [41]. The two inequivalent planes are separated by Sn_3 and Sn_2Y layers. The Mn planes separated by Sn_3 are slightly larger in distance than Mn planes separated by Sn_2Y . Because of this unique structural feature, the magnetic properties of YMn_6Sn_6 are very sensitive to both the distance between Mn-Mn along the c -axis and the nature of R element in the series of RMn_6Sn_6 (R=rare earth element). The isotropic Heisenberg exchange interactions J_{ij} 's have been calculated without and with SOC using different density functionals

like spin polarized local density approximation (LSDA) and general gradients approximation (GGA) which follow a long-ranged Ruderman-Kittel-Kasuya-Yosida (RKKY) coupling [41]. The full mapping of Mn-Mn magnetic exchanges in YMn_6Sn_6 for nearest neighbours are presented in the Fig.1(a)-(b) along in-plane (ab -plane) and out of plane (c -axis) directions respectively. ab -plane Mn-Mn interaction (J_1) is strongly FM whereas the Mn-Mn interactions along the c -axis are markedly different following the AFM (J_2) coupling across the Sn_2Y layer and FM exchange interaction (J_3) across the Sn_3 layer.

To describe the exchange interactions in more efficient way, we took $1 \times 1 \times 2$ supercell of YMn_6Sn_6 as a smallest possible magnetic unit cell which contains 4 Mn kagome planes following AFM coupling across Sn_2Y layer and FM coupling across the Sn_3 layer. The total magnetic exchange interactions in YMn_6Sn_6 are long ranged and can be categorized into two sets. One is in the kagome plane (ab -plane) and other one is along the c -axis. The Heisenberg magnetic exchange interactions in the kagome plane (denoted by J_{ip} for $i=1, 2, 3$) are J_{1p} (J_1), J_{2p} (J_4), J_{3p} (J_7) and along the c -axis (denoted by J_{ic} for $i=1, 2, 3, 4, 5$) are J_{1c} (J_2), J_{2c} (J_3), J_{3c} (J_{16}), J_{4c} (J_n), J_{5c} (J_m) as shown in the Fig.1(a)-(b) [41].

Calculated magnetic exchange interactions for YMn_6Sn_6 are shown in the Fig. 1(c). The in-plane Mn atoms have strong FM interaction ($J_{1p} = 3.34$ meV). The isotropic Heisenberg exchange interactions along the c -axis (J_{ic} for $i=1, 2, 3, 4, 5$) are -11.74, 8.66, -1.61, -0.37 and -1.23 meV respectively. The inter and intra Mn-Mn layers have AFM (J_{1c}) and FM (J_{2c}) coupling respectively, whereas the intra and inter bilayers have AFM (J_{3c}) coupling. The next inter (J_{4c}) and intra (J_{5c}) bilayers both have AFM coupling. But the magnetic exchange interaction between Mn layers separated by Sn_3 layer are interacting FM (J_{2c}). Therefore, competition between the J_{2c} (FM) and J_{4c} (AFM) leads to frustration in the structural geometry and a complex magnetic ground state in YMn_6Sn_6 [41]. We will discuss in the subsequent section. The calculated magnetic moment is $2.36 \mu_B/\text{Mn}$ from LSDA.

Both the LDA and GGA fail to capture the magnetic exchange interactions accurately containing d-orbitals compared to experimental report [39, 41] which requires the treatment of inclusion of Hubbard U on Mn-3d state. Figure 1(c) shows the isotropic Heisenberg interactions J_{ij} 's with the inclusion of Hubbard U on Mn-3d orbital. LDA+U affects both the in-plane (ab -plane) and out of plane (along c -axis) magnetic exchanges in YMn_6Sn_6 . J_{1p} increases with increasing the strength of Hubbard U on Mn-3d state. The calculated in-plane (J_{1p}) and out of plane magnetic exchange interactions along the c -axis (J_{ic} for $i=1, 2, 3, 4, 5$) are 10.59 meV, and -8.01, 7.09, -1.21, -0.49, -1.07 meV respectively with Hubbard U = 2 eV. The remarkable difference in the Heisenberg exchange interactions with inclusion of Hubbard U is that intra layer FM coupling (J_{2c}) decreases and next inter bilayer AFM coupling (J_{4c}) increases respectively which

enhances frustration in the out of plane magnetic exchanges. However, J_{1p} and J_{1c} , J_{2c} , J_{3c} , J_{4c} , J_{5c} , are 17.61 meV and -4.51, 3.01 -0.66, -0.33, -0.45 meV respectively from LSDA+U with a Hubbard $U = 3$ eV. The calculated magnetic moment is 2.26 (2.21) μ_B/Mn from LSDA+U with $U = 2$ (3) eV.

The correlation effects among the localised Mn-3d electrons play an important role in the kagome lattice. This motivate us to use a combination of DFT and dynamical mean-field theory (DMFT) with inclusion of Hubbard U on Mn-3d state to describe the electronic structure properly. We used the LSDA functional and spin-polarized T-matrix fluctuation impurity solver to accurately capture the magnetic exchanges as shown in Fig.1(c) (for $U = 2$ and 3 eV respectively). J_{1p} and J_{1c} , J_{2c} , J_{3c} , J_{4c} , J_{5c} , are 5.49 meV and -11.13, 7.81, -1.49, -0.69, -1.22 meV respectively from LSDA+DMFT with a Hubbard $U = 2$ eV. However, J_{1p} and J_{1c} , J_{2c} , J_{3c} , J_{4c} , J_{5c} , are 4.85 meV and -9.17, 8.61, -1.18, -0.02, -0.65 meV respectively from LSDA+DMFT with a Hubbard $U = 3$ eV. How J_{ic} 's affect the spin texture for the magnetic ground state of YMn_6Sn_6 that will be discussed in the subsequent section. The calculated magnetic moment is 2.29 (2.23) μ_B/Mn from LSDA+DMFT with $U = 2$ (3) eV is in excellent agreement with experimental report [39].

Symmetric Heisenberg exchanges J_{ij} 's indulge collinear ordering whereas the anti-symmetric DMI's (D_{ij} 's) cant the spin favouring the non-collinear magnetic ground state. Figure 1(d) show DMI for YMn_6Sn_6 . $D_1(D_{1p})$ increases whereas $D_4(D_{2p})$ has a continuous decreasing trends with increasing Hubbard U . The inter ($D_2 = D_{1c}$) and intra layer ($D_3 = D_{2c}$) DMIs are zero. The components DMIs along the in-plane (ab -plane) and out of plane (c -axis) directions for D_{1p} are $D_{1p}^{\parallel} \sim 0.251(0.218)$ meV and $D_{1p}^z \sim 0$ meV respectively from LSDA+DMFT with $U = 2$ (3) eV. Whereas they are $D_{2p}^{\parallel} \sim 0.068(0.046)$ meV and $D_{2p}^z \sim 0.455(0.308)$ meV for D_{2p} respectively as shown in Fig.1(d).

Frustration driven spin spiral : Capturing spin texture in the magnetic ground state of a frustrated 3D kagome lattice like YMn_6Sn_6 is a real challenge and needs assiduous attention. The system consists of stacking of FM kagome planes where the frustration in magnetic exchanges come from the next inter bilayer couplings (J_{4c}). Real-space magnetic configurations are confirmed by both Monte carlo (MC) simulations and spin dynamics (SD) simulation as implemented in UppASD code [42] with the spin Hamiltonian given by :

$$H = - \sum_{i,j} J_{ij} \mathbf{S}_i \cdot \mathbf{S}_j - \sum_{i,j} \mathbf{D}_{ij} \cdot (\mathbf{S}_i \times \mathbf{S}_j) - \sum_i K(S_i^z)^2,$$

Where K is the magnetic anisotropic energy. The calculated magnetic anisotropy energy ($E_c - E_p$) for YMn_6Sn_6 is ~ 0.05 meV from LSDA+DMFT with Hubbard $U = 2$ eV which is below to the experimental report (~ 0.2 meV) [37].

We simulate a finite-sized 3D kagome slab having dimension with $96 \times 96 \times 31$ with periodic boundary condi-

tions. Efficient thermalization is guaranteed by simulated temperature annealing where the both the MC and SD simulations are started from a random spin configuration corresponding to high temperature 1000 K until the lowest temperature 10^{-5} K is reached. Raising the temperature randomizes spin orientation due to thermal fluctuations to avoid any specific magnetic order. At each temperature, we used 2×10^5 MC sweeps for equilibration, and 5×10^5 MC sweeps (in time steps of steps of 1000 MC sweeps and in time steps 10^{-16} sec) for the measurement of physical observable. In order to search a correct magnetic ground state, metastable states at the low-temperature regime are avoided by starting the simulation from a variational ground state and then increasing the temperature using the MC scheme. We used the magnetic exchanges and DMI parameters for the spin Hamiltonian from three different calculation schemes like LSDA, LSDA with Hubbard $U = 2, 3$ eV and DFT+DMFT with Hubbard $U = 2, 3$ eV respectively.

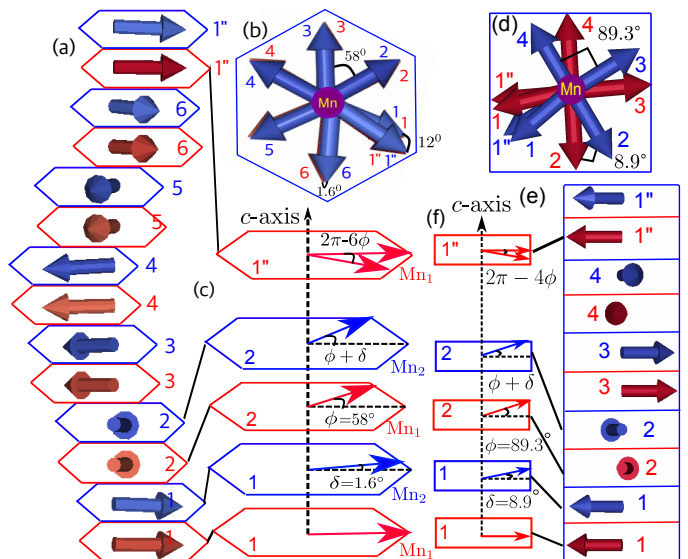


FIG. 2. (a) Side and (b) top view of two incommensurate spin spirals (SS) propagating along c -axis marked by two different colors from spin dynamics simulation with magnetic interactions from LSDA+DMFT with $U = 2$ eV. The SS repeats after 6.19 Mn layers marked by numbers. (c) Schematic representation of two SSs with an angle $\delta \sim 1.6^\circ$ between them and showing the pitch angle ($\phi \sim 58^\circ$), and incommensurate angle ($2\pi - 6\phi \sim 12^\circ$). (d) Side, (e) top view and (f) schematic representation of the same SSs with magnetic interactions from LSDA+DMFT with $U = 3$ eV. Here the pitch angle ϕ and δ are 89.3° and 8.9° respectively. The incommensurate angle reduces to $2\pi - 4\phi$ ($\sim 3^\circ$) repeating after 4.03 Mn layers.

Figure 2(a)-(b) shows the spin texture of magnetic ground state of YMn_6Sn_6 from LSDA+DMFT with $U = 2$ eV within full relativistic limit. The magnetic ground state of YMn_6Sn_6 is a combination of two incommensurate SSs along the c -axis with a wave vector $\mathbf{q} \sim (0 \ 0 \ 0.1615)$ and has a rotational plane along $[001]$. The in-

commensurate spiral phase has been reported in separate experimental studies [35–39], but demands the theoretical inspection from a combination of full first principles and spin dynamics approach for the prediction of correct magnetic ground state. The two incommensurate spirals (marked by blue and red colours in the Fig.2(a)-(b)) correspond to two different Mn kagome planes as described in the magnetic crystal structure of YMn_6Sn_6 [41]. The two adjacent moment layers belonging to two different Mn kagome planes are coupled FM with an angle $\delta \sim 1.6^\circ$ which is basically the angle between two incommensurate SSs as shown in Fig.2(b)-(c).

Now we analyse the spin texture layer by layer. Figure 2(a) and (b) show layer and top view spin texture of two incommensurate SSs respectively. The two incommensurate SSs form by a combination of two cycloidal SSs (also called double fan like structure [43]). The spin arrangements in each incommensurate SS repeats after 6.19 Mn layers along the c -axis marked by numbering in two different colours as shown in the Fig.2(a)-(b) with a small incommensurate angle. The pitch angle (ϕ) and incommensurate angle ($2\pi - 6\phi$) in each cycloidal SS or fan moment in this double-fan like structure are $\sim 58^\circ$ and $\sim 12^\circ$ respectively.

The SSs in YMn_6Sn_6 are sensitive on the choice of Hubbard U on Mn-3d orbitals. The pitch angle and δ of two incommensurate SSs increase to $\sim 89.3^\circ$ and $\sim 8.9^\circ$ if we increase the Hubbard U on Mn-3d orbitals to 3 eV in LSDA+DMFT as shown in Fig.2(d)-(f). The spin arrangements in each incommensurate SS repeats after 4.03 Mn layers with LSDA+DMFT with a Hubbard $U = 3$ eV. Here the incommensurate angle ($2\pi - 4\phi$) and wave vector (\mathbf{q}) for each cycloidal SS are $\sim 3^\circ$ and $\sim (0 \ 0 \ 0.248)$ respectively which is good agreement with the experimental reports [18, 38–40].

We also studied the effects of anisotropic energy on the incommensurate SS within relativistic limit. The anisotropic energy flips the rotational plane of double-fan structure from $[1\bar{1}0]$ to $[001]$ and locks it in ab -plane. The incommensurate SS is not DMI induced, rather it is inter bilayer frustration enforced. The effect of exchange frustration is less in magnetic interactions calculated from LSDA. Therefore, LSDA gives a FM ground state consisting of AFM block with 4 Mn layers along the c -axis where Mn kagome planes separated by Sn_2Y and Sn_3 have AFM and FM spin arrangements respectively [41]. Inclusion of a small Hubbard $U \sim (2\text{-}3$ eV has a tendency of forming SS along the c -axis [41].

The root of the spin reorientation will be discussed in the next section within the framework of nearest neighbour magnetic exchange interactions along the c -axis (J_{ic} for $i=2, 4$). YMn_6Sn_6 is three dimensional (3D) kagome metal of having long range RKKY interactions where magnetic exchanges along c -axis play the main role of predicting the complex magnetic ground state. The in-plane magnetic exchanges in kagome plane are always interacting ferromagnetically. The inter and next intra bilayer magnetic exchanges in YMn_6Sn_6 are $J_{2c} \sim$

8.66 meV and $J_{4c} \sim -0.37$ meV respectively from LSDA. Whereas the corresponding values are $J_{2c} \sim 8.61$ (7.81) meV and $J_{4c} \sim -0.02$ (-0.69) meV from LSDA+DMFT with a Hubbard $U = 3$ (2) eV. The competition between J_{2c} and J_{4c} tends to form two SSs with a plane of rotation along $[001]$ [41]. It gives two incommensurate SSs with a pitch angle $\phi \sim 89.3^\circ$ (58°) and $\delta \sim 8.9^\circ$ (1.6°) with LSDA+DMFT with a Hubbard $U = 3$ (2) eV where anisotropy energy fastens the SS strongly in the kagome plane of YMn_6Sn_6 as shown in Fig.2. Putting $J_{4c} \sim 0$, the pitch angle ϕ remains same but the angle between two incommensurate SSs δ increases to $\sim 11^\circ$ (± 0.2). The out of plane magnetic exchanges for YMn_6Sn_6 are $J_{2c} \sim 3.01$ (7.09) meV and $J_{4c} \sim -0.33$ (-0.49) meV from LSDA+ U with $U = 3$ (2) eV. However, the pitch angle ϕ of the incommensurate SS is 102° ($\sim 54^\circ$) from LSDA+ U with $U = 3$ (2) eV respectively.

Effective Hamiltonian for incommensurate SSs : Spin dynamics simulation fails to capture the experimentally observed two non-equivalent SS with slightly different pitch angles [37]. Therefore, we consider an effective model Hamiltonian for the two incommensurate SSs considering total the magnetic exchange interactions (called it an effective exchanges) within Mn planes along c -axis (J_{ic}^{eff} with $i=1,2,3,4,5$) [41] to study the effect of Hubbard U on SSs of YMn_6Sn_6 and is given by :

$$H_{ic}^{eff} = -J_{1c}^{eff} \cos(\phi - \delta) - J_{2c}^{eff} \cos \delta - 2J_{3c}^{eff} \cos \phi - J_{4c}^{eff} \cos(2\phi - \delta) - J_{5c}^{eff} \cos(\phi + \delta)$$

Such qualitative considerations allow us to understand

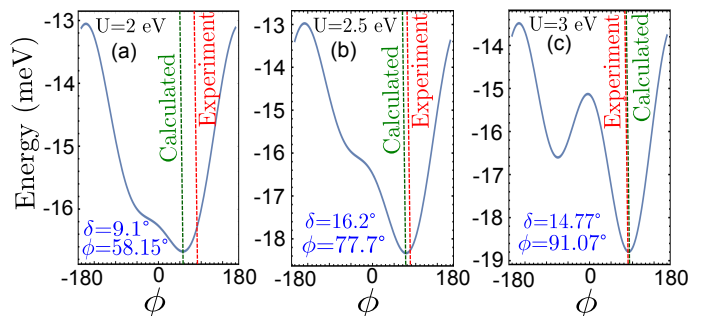


FIG. 3. Calculated variation of energy with the pitch angle from LSDA+DMFT with (a) $U = 2$ eV, (b) $U = 2.5$ eV and (c) $U = 3$ eV respectively. The calculated pitch angles are compared with experimental report [37].

the detail root of arising SS in the YMn_6Sn_6 and evolution of pitch angles of two incommensurate SSs with correlation. The effective magnetic interactions within Mn planes along the c -axis are interacting FM which leads to a FM ground state from LSDA calculations ($\phi = 0, \delta = 0$) [41]. The inclusion of Hubbard U on Mn-3d orbitals leads to SS magnetic ground state from FM for both LSDA+ U and LSDA+DMFT. We scan the magnetic ground state of YMn_6Sn_6 with different Hubbard U parameters ranging from $U = (1\text{-}4)$ eV (see table II in supplementary

material) [41]. YMn_6Sn_6 remains in spiral phase with $U = (2-3)$ eV and remains in FM phase otherwise. Figure 3(a)-(c) represent the energy evolution of SS with pitch angle with Hubbard $U = 2, 2.5, 3$ eV respectively. The asymmetric double well nature of energy with pitch angles confirms the signature of two non-equivalent and incommensurate SSs in YMn_6Sn_6 . The calculated pitch angle for the dominant SS $\phi \sim 91^\circ$ matches with the experimental reports [18, 38–40] which is also in good agreement with the simulated SS ($\phi \sim 89^\circ$) obtained from LSDA+DMFT with $U = 3$ eV.

In order to understand the effect of correlation on incommensurate SS, we analyse the effective magnetic exchanges (J_{ic}^{eff} 's) with different Hubbard U . $J_{1c}^{eff}, J_{2c}^{eff}$ are FM whereas J_{3c}^{eff} is AFM always. Now exchange frustration in YMn_6Sn_6 comes from $J_{3c}^{eff}, J_{4c}^{eff}$ when they switch into AFM from FM with gradually increasing Hubbard U on Mn-3d orbital (see table II in supplementary material) [41]. The inclusion of Hubbard $U = 2$ eV flips J_{4c}^{eff} to AFM (-0.54 meV) from FM but J_{3c}^{eff} remains FM (0.13 meV). This leads to frustration in the magnetic exchanges of YMn_6Sn_6 and gives magnetic ground state a combination of two incommensurate SSs with $\phi = 58.15^\circ$, $\delta = 9.1^\circ$. The exchange frustration increases with $U=2.5$ eV and J_{3c}^{eff} flips into AFM (-0.34 meV) from FM which increase both the pitch angle ϕ and δ to 77.7° and 16.2° respectively. YMn_6Sn_6 gives SS with $\phi = 91.07^\circ$ and $\delta = 14.77^\circ$ in presence of $U = 3$ eV where J_{3c}^{eff} (-1.32 meV) and J_{4c}^{eff} (-1.62 meV) are strongly AFM as shown in Fig. 3(c).

Topology in magnon: The kagome lattice provides an ideal system to investigate topological magnon. AFM kagome lattice exhibits a flat spin wave mode due to geometrical spin frustration [44] whereas a flat mode also exists in a FM kagome [45]. However, the topological investigation in kagome SS has pending yet. We calculated the magnon bands along the high symmetry $\Gamma-K-M-\Gamma$ direction from LSDA+DMFT without and with SOC. Two Dirac crossings (Dirac magnons) appear at 85 and 108 meV (with $U = 3$ eV) at high symmetry K point without SOC where the bands are doubly degenerated. However, the two Dirac points appear slightly below at 73 and 100 meV with $U = 2$ eV [41]. To compare with calculated magnon spectra with another experimental study reported by Zhang et al. [39], we calculated the dynamical structure factor $S(\mathbf{q}, \omega)$ from spin dynamics simulation at $T = 5$. $S(\mathbf{q}, \omega)$ is proportional to the inelastic scattering intensity which is in good agreement with the experimental measured spectra by Zhang et al. [39] with LSDA+DMFT with $U = 2$ eV [41].

Figure 4(a) shows the magnon bands of YMn_6Sn_6 where the magnetic ground state is a admixture of two incommensurate SSs. We can categorized the total bands into three sets (upper, middle and lower bands) coming from three distinct magnon bands in kagome lattice. The degeneracies at K point (Dirac crossings) have broken with inclusion of DMI (with SOC) and two topological

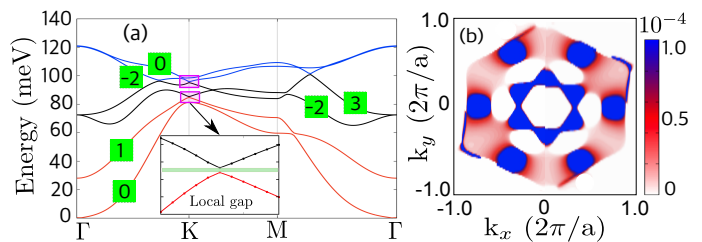


FIG. 4. (a) Magnon bands with calculated Chern numbers and (b) Berry curvature profile in YMn_6Sn_6 with SOC. Topological gaps are marked by boxes in figure (a).

gap (topological magnon) appear at that point. One gap is of 0.52 meV around 84 meV and other is of 0.64 meV around 95 meV (marked by boxes in Fig.4(a)). Similar to magnon, we also observed Dirac points which open gap in presence of SOC and flat bands near the Fermi level in the electronic band structure of YMn_6Sn_6 [41].

Our findings are further corroborated by calculating the topological invariants for acid testing of the existence of topological magnon in YMn_6Sn_6 . There exist no global gap in magnon bands as the maximum of the each band is higher in energy than the minimum of its next magnon band. Therefore, one can define the Chern numbers considering local gaps around the high symmetry K point in Brillouin zone (BZ) where topological gap appear [46–48]. The calculated Chern numbers are 0, 1, -2, 3, -2, 0 respectively as shown in the Fig.4(a). We got the maximum Chern number $c = -2$ for upper magnon band belonging to flat band of kagome lattice as the number of Mn kagome planes in an unit cell is 2 [49]. Figure 4(b) shows the calculated Berry curvature profile. Here the maxima appears at high symmetry K point where the topological gap appears in BZ. This is another signature of existing topological magnon in kagome SS of YMn_6Sn_6 .

We further investigate the effects of DMI's on the existence of topological magnon considering an quasi 2D structure of YMn_6Sn_6 . Here consider only in-plane (ab -plane) magnetic interactions (J_{ip}, D_{ip} for $i=1, 2$ as both D_{1c} and D_{2c} are 0) on topological magnons. The topological insulating phase in kagome magnet switches into gapless topological mode for quasi 2D structure ($\frac{D_{1p}^z}{J_{1p}} \sim 0$) [41] which opens a gap with inclusion of $D_{2p}^z \neq 0$. Therefore, opening of two topological gaps shown in Fig. 4(a) are mainly attributed by the $D_{2p}^z \neq 0$ as $D_{1p}^z \sim 0$. However, ab -plane magnetic interactions (J_{ip}, D_{ip}) within a kagome plane play the governing role in producing the topological magnon whereas the magnetic exchanges along the c -axis (J_{ic}) introduce incommensurate SS phase in YMn_6Sn_6 .

Conclusion and outlook : We demonstrate the reorientation of spin texture from the FM state into two incommensurate SSs in YMn_6Sn_6 due to next inter bilayer magnetic exchange frustration. YMn_6Sn_6 has a FM ground state from DFT approach, whereas has a SS phase from

DFT+DMFT+U approach. The reason for this discrepancy in predicting experimental ground stems from the failure of DFT to capture the effect of electronic correlations. We propose a model Hamiltonian for two incommensurate SS to explain FM-SS crossover due to AFM spin exchange with correlation. We reported the topological magnon in the kagome SS of YMn_6Sn_6 emerging from in-plane magnetic exchanges. Additionally, we observed DPs and flat bands near the Fermi level in the electronic structure of YMn_6Sn_6 . Our study provides a detailed platform to understand the influence of the out of plane Heisenberg exchange interactions on the behaviour of incommensurate SSs, and DMIs stemming from the Mn-based kagome planes on topological magnon respectively. The interplay between magnetic structure and topology in both fermions (spin) and bosons (magnon) makes YMn_6Sn_6 as an ideal candidate to study the topological Hall transport in future [22, 34, 40, 50, 51].

ACKNOWLEDGMENTS

BS would like to thank H. Zhang for providing the experimental cif file, Y. O. Kvashnin and I. Miranda for fruitful discussions. Financial support from Vetenskapsrådet (grant numbers VR 2016-05980 and VR 2019-05304), and the Knut and Alice Wallenberg foundation (grant numbers KAW 2018.0060, KAW 2021.0246, and KAW 2022.0108) is acknowledged. A.B. acknowledges eSSSENCE. The computations were enabled by resources provided by the National Academic Infrastructure for Supercomputing in Sweden (NAISS) and the Swedish National Infrastructure for Computing (SNIC) at NSC and PDC, partially funded by the Swedish Research Council through grant agreements no. 2022-06725 and no. 2018-05973.

-
- [16] Tian-Heng Han, Joel S. Helton, Shaoyan Chu, Daniel G. Nocera, Jose A. Rodriguez-Rivera, Collin Broholm, and Young S. Lee, “Fractionalized excitations in the spin-liquid state of a kagome-lattice antiferromagnet,” *Nature* **492**, 406–410 (2012).
- [17] Kenya Ohgushi, Shuichi Murakami, and Naoto Nagaosa, “Spin anisotropy and quantum hall effect in the kagomé lattice: Chiral spin state based on a ferromagnet,” *Phys. Rev. B* **62**, R6065–R6068 (2000).
- [18] Nirmal J Ghimire and Igor I Mazin, “Topology and correlations on the kagome lattice,” *Nature Materials* **19**, 137–138 (2020).
- [19] Yi Zhou, Kazushi Kanoda, and Tai-Kai Ng, “Quantum spin liquid states,” *Rev. Mod. Phys.* **89**, 025003 (2017).
- [20] Tian-Heng Han, Joel S Helton, Shaoyan Chu, Daniel G Nocera, Jose A Rodriguez-Rivera, Collin Broholm, and Young S Lee, “Fractionalized excitations in the spin-liquid state of a kagome-lattice antiferromagnet,” *Nature* **492**, 406–410 (2012).
- [21] Jia-Xin Yin, Songtian S. Zhang, Guoqing Chang, Qi Wang, Stepan S. Tsirkin, Zurab Guguchia, Biao Lian, Huibin Zhou, Kun Jiang, Ilya Belopolski, Nana Shumiya, Daniel Multer, Maksim Litskevich, Tyler A. Cochran, Hsin Lin, Ziqiang Wang, Titus Neupert, Shuang Jia, Hechang Lei, and M. Zahid Hasan, “Negative flat band magnetism in a spin-orbit-coupled correlated kagome magnet,” *Nature Physics* **15**, 443–448 (2019).
- [22] Enke Liu, Yan Sun, Nitesh Kumar, Lukas Muechler, Aili Sun, Lin Jiao, Shuo-Ying Yang, Defa Liu, Aiji Liang, Qiunan Xu, Johannes Kroder, Vicky Süß, Horst Borrmann, Chandra Shekhar, Zhaosheng Wang, Chuanying Xi, Wenhong Wang, Walter Schnelle, Steffen Wirth, Yulin Chen, Sebastian T. B. Goennenwein, and Claudia Felser, “Giant anomalous hall effect in a ferromagnetic kagome-lattice semimetal,” *Nature Physics* **14**, 1125–1131 (2018).
- [23] Mingu Kang, Linda Ye, Shiang Fang, Jhih-Shih You, Abe Levitan, Minyong Han, Jorge I. Facio, Chris Jozwiak, Aaron Bostwick, Eli Rotenberg, Mun K. Chan, Ross D. McDonald, David Graf, Konstantine Kaznatcheev, Elio Vescovo, David C. Bell, Efthimios Kaxiras, Jeroen van den Brink, Manuel Richter, Madhav Prasad Ghimire, Joseph G. Checkelsky, and Riccardo Comin, “Dirac fermions and flat bands in the ideal kagome metal fesn_3 ,” *Nature Materials* **19**, 163–169 (2020).
- [24] J-X Yin, Nana Shumiya, Sougata Mardanya, Qi Wang, Songtian S Zhang, Hung-Ju Tien, Daniel Multer, Yuxiao Jiang, Guangming Cheng, Nan Yao, Shangfei Wu, Desheng Wu, Liangzi Deng, Zhipeng Ye, Rui He, Guoqing Chang, Zhonghao Liu, Kun Jiang, Ziqiang Wang, Titus Neupert, Amit Agarwal, Tay-Rong Chang, Ching-Wu Chu, Hechang Lei, and M Zahid Hasan, “Fermion-boson many-body interplay in a frustrated kagome paramagnet,” *Nature Communications* **11**, 4003 (2020).
- [25] Yang Zhang, Yan Sun, Hao Yang, Jakub Železný, Stuart P. P. Parkin, Claudia Felser, and Binghai Yan, “Strong anisotropic anomalous hall effect and spin hall effect in the chiral antiferromagnetic compounds mn_3x ($x = \text{Ge}, \text{sn}, \text{ga}, \text{ir}, \text{rh}, \text{and pt}$),” *Phys. Rev. B* **95**, 075128 (2017).
- [26] Pyeongjae Park, Joosung Oh, Klára Uhlířová, Jerome Jackson, András Deák, László Szunyogh, Ki Hoon Lee, Hwanbeom Cho, Ha-Leem Kim, Helen C Walker, Devashibhai Adroja, Vladimír Sechovský, and Je-Geun Park, “Magnetic excitations in non-collinear antiferromagnetic weyl semimetal Mn_3Sn ,” *npj Quantum Materials* **3**, 63 (2018).
- [27] Yutaro Takeuchi, Yuta Yamane, Ju-Young Yoon, Ryuichi Itoh, Butsurin Jinnai, Shun Kanai, Jun’ichi Ieda, Shunsuke Fukami, and Hideo Ohno, “Chiral-spin rotation of non-collinear antiferromagnet by spin-orbit torque,” *Nature Materials* **20**, 1364–1370 (2021).
- [28] Dongwook Go, Moritz Sallermann, Fabian R Lux, Stefan Blügel, Olena Gomonay, and Yuriy Mokrousov, “Non-collinear spin current for switching of chiral magnetic textures,” *arXiv preprint arXiv:2201.11476* (2022).
- [29] S. Sinnema, R.J. Radwanski, J.J.M. Franse, D.B. de Mooij, and K.H.J. Buschow, “Magnetic properties of ternary rare-earth compounds of the type $\text{r}_2\text{fe}_{14}\text{b}$,” *Journal of Magnetism and Magnetic Materials* **44**, 333–341 (1984).

- [30] M.S.S. Brooks, L. Nordström, and B. Johansson, “Rare-earth transition-metal intermetallics,” *Physica B: Condensed Matter* **172**, 95–100 (1991).
- [31] B. Malaman, G. Venturini, R. Welter, J.P. Sanchez, P. Vulliet, and E. Ressouche, “Magnetic properties of RMn₆Sn₆ (R=Gd–Er) compounds from neutron diffraction and mössbauer measurements,” *Journal of Magnetism and Magnetic Materials* **202**, 519–534 (1999).
- [32] D.M Clatterbuck and K.A Gschneidner, “Magnetic properties of RMn₆Sn₆ (R=Tb, Ho, Er, Tm, Lu) single crystals,” *Journal of Magnetism and Magnetic Materials* **207**, 78–94 (1999).
- [33] Jia-Xin Yin, Wenlong Ma, Tyler A Cochran, Xitong Xu, Songtian S Zhang, Hung-Ju Tien, Nana Shumiya, Guangming Cheng, Kun Jiang, Biao Lian, Zhida Song, Guoqing Chang, Ilya Belopolski, Daniel Multer, Maksim Litskevich, Zi-Jia Cheng, Xian P Yang, Bianca Swidler, Huibin Zhou, Hsin Lin, Titus Neupert, Ziqiang Wang, Nan Yao, Tay-Rong Chang, Shuang Jia, and M Zahid Hasan, “Quantum-limit chern topological magnetism in TbMn₆Sn₆,” *Nature* **583**, 533–536 (2020).
- [34] Wenlong Ma, Xitong Xu, Zihe Wang, Huibin Zhou, Madalynn Marshall, Zhe Qu, Weiwei Xie, and Shuang Jia, “Anomalous hall effect in the distorted kagome magnets (Nd,Sm)Mn₆Sn₆,” *Phys. Rev. B* **103**, 235109 (2021).
- [35] Rebecca L. Dally, Jeffrey W. Lynn, Nirmal J. Ghimire, Dina Michel, Peter Siegfried, and Igor I. Mazin, “Chiral properties of the zero-field spiral state and field-induced magnetic phases of the itinerant kagome metal YMn₆Sn₆,” *Phys. Rev. B* **103**, 094413 (2021).
- [36] Qi Wang, Kelly J. Neubauer, Chunruo Duan, Qiangwei Yin, Satoru Fujitsu, Hideo Hosono, Feng Ye, Rui Zhang, Songxue Chi, Kathryn Krycka, Hechang Lei, and Pengcheng Dai, “Field-induced topological hall effect and double-fan spin structure with a *c*-axis component in the metallic kagome antiferromagnetic compound YMn₆Sn₆,” *Phys. Rev. B* **103**, 014416 (2021).
- [37] Nirmal J. Ghimire, Rebecca L. Dally, L. Poudel, D. C. Jones, D. Michel, N. Thapa Magar, M. Bleuel, Michael A. McGuire, J. S. Jiang, J. F. Mitchell, Jeffrey W. Lynn, and I. I. Mazin, “Competing magnetic phases and fluctuation-driven scalar spin chirality in the kagome metal YMn₆Sn₆,” *Science Advances* **6**, eabe2680 (2020), <https://www.science.org/doi/pdf/10.1126/sciadv.abe2680>.
- [38] EV Rosenfeld and NV Mushnikov, “Double-flat-spiral magnetic structures: Theory and application to the RMn₆X₆ compounds,” *Physica B: Condensed Matter* **403**, 1898–1906 (2008).
- [39] H. Zhang, X. Feng, T. Heitmann, A. I. Kolesnikov, M. B. Stone, Y.-M. Lu, and X. Ke, “Topological magnon bands in a room-temperature kagome magnet,” *Phys. Rev. B* **101**, 100405 (2020).
- [40] C. Q. Xu, T. W. Heitmann, H. Zhang, Xiaofeng Xu, and X. Ke, “Magnetic phase transition, magnetoresistance, and anomalous hall effect in Ga-substituted YMn₆X₆ with a ferromagnetic kagome lattice,” *Phys. Rev. B* **104**, 024413 (2021).
- [41] See supplemental materials xxxx-xxxx for the discussion on the following sections : “Theoretical and computational details”; and “Crystal structure of YMn₆Sn₆”; and “Magnetic interactions”; and “Spin textures from both spin dynamics simulationa and effective model Hamiltonian”; and “Magnon band structure”; and “Electronic band structure” of YMn₆Sn₆”.
- [42] [Http://github.com/UppASD/UppASD](http://github.com/UppASD/UppASD).
- [43] David C. Johnston, “Magnetic structure and magnetization of helical antiferromagnets in high magnetic fields perpendicular to the helix axis at zero temperature,” *Phys. Rev. B* **96**, 104405 (2017).
- [44] K. Matan, D. Grohol, D. G. Nocera, T. Yildirim, A. B. Harris, S. H. Lee, S. E. Nagler, and Y. S. Lee, “Spin waves in the frustrated kagomé lattice antiferromagnet kfe₃(OH)₆(so₄)₂,” *Phys. Rev. Lett.* **96**, 247201 (2006).
- [45] R. Chisnell, J. S. Helton, D. E. Freedman, D. K. Singh, R. I. Bewley, D. G. Nocera, and Y. S. Lee, “Topological magnon bands in a kagome lattice ferromagnet,” *Phys. Rev. Lett.* **115**, 147201 (2015).
- [46] Sebastián A. Díaz, Jelena Klinovaja, and Daniel Loss, “Topological magnons and edge states in antiferromagnetic skyrmion crystals,” *Phys. Rev. Lett.* **122**, 187203 (2019).
- [47] Wanxiang Feng, Di Xiao, Jun Ding, and Yugui Yao, “Three-dimensional topological insulators in I–III–v₂ and II–IV–v₂ chalcopyrite semiconductors,” *Phys. Rev. Lett.* **106**, 016402 (2011).
- [48] Surasree Sadhukhan, Banasree Sadhukhan, and Sudipta Kanungo, “Pressure-driven tunable properties of the small-gap chalcopyrite topological quantum material zn₂sb₂: A first-principles study,” *Phys. Rev. B* **106**, 125112 (2022).
- [49] Maximilian Trescher and Emil J. Bergholtz, “Flat bands with higher chern number in pyrochlore slabs,” *Phys. Rev. B* **86**, 241111 (2012).
- [50] Banasree Sadhukhan and Tanay Nag, “Effect of chirality imbalance on hall transport of prrh₂,” *Phys. Rev. B* **107**, L081110 (2023).
- [51] Alexander Mook, Jürgen Henk, and Ingrid Mertig, “Magnon hall effect and topology in kagome lattices: A theoretical investigation,” *Phys. Rev. B* **89**, 134409 (2014).
- [52] A Il Liechtenstein, MI Katsnelson, VP Antropov, and VA Gubanov, “Local spin density functional approach to the theory of exchange interactions in ferromagnetic metals and alloys,” *Journal of Magnetism and Magnetic Materials* **67**, 65–74 (1987).
- [53] M. I. Katsnelson and A. I. Lichtenstein, “First-principles calculations of magnetic interactions in correlated systems,” *Phys. Rev. B* **61**, 8906–8912 (2000).
- [54] VP Antropov, MI Katsnelson, and AI Liechtenstein, “Exchange interactions in magnets,” *Physica B: Condensed Matter* **237**, 336–340 (1997).
- [55] L. Udvardi, L. Szunyogh, K. Palotás, and P. Weinberger, “First-principles relativistic study of spin waves in thin magnetic films,” *Phys. Rev. B* **68**, 104436 (2003).
- [56] H. Ebert and S. Mankovsky, “Anisotropic exchange coupling in diluted magnetic semiconductors: Ab initio spin-density functional theory,” *Phys. Rev. B* **79**, 045209 (2009).
- [57] Andrea Secchi, Alexander I Lichtenstein, and Mikhail I Katsnelson, “Magnetic interactions in strongly correlated systems: Spin and orbital contributions,” *Annals of Physics* **360**, 61–97 (2015).
- [58] Man Li, Qi Wang, Guangwei Wang, Zhihong Yuan, Wenhua Song, Rui Lou, Zhengtai Liu, Yaobo Huang, Zhonghao Liu, Hechang Lei, Zhiping Yin, and Shancai Wang, “Dirac cone, flat band and saddle point in kagome magnet YMn₆Sn₆,” *Nature Communications* **12**,

3129 (2021).

Supplementary material for “Topological magnon in exchange frustration driven incommensurate spin spiral of a kagome lattice YMn_6Sn_6 ”

Banasree Sadhukhan,^{1,2} Anders Bergman,³ Patrik Thunström,³ Manuel Pereiro Lopez³, Olle Eriksson,³ Anna Delin,^{2,4,5}

¹*Department of Physics and Nanotechnology, SRM Institute of Science and Technology, Kattankulathur, 603203, Chennai, Tamil Nadu, India*

²*Department of Applied Physics, School of Engineering Sciences, KTH Royal Institute of Technology, AlbaNova University Center, SE-10691 Stockholm, Sweden*

³*Department of Physics and Astronomy, Uppsala University, Box 516, SE-75120 Uppsala, Sweden*

⁴*Swedish e-Science Research Center (SeRC), KTH Royal Institute of Technology, SE-10044 Stockholm, Sweden*

⁵*Wallenberg Initiative Materials Science for Sustainability (WISE), KTH Royal Institute of Technology, SE-10044 Stockholm, Sweden*

I. THEORETICAL AND COMPUTATIONAL DETAILS

A. Magnetic interactions

The density functional theoretical (DFT) calculations for both the electronic structures and the magnetic interactions are performed within full-potential linear muffin-tin orbital-based code RSPt [1] using both local spin density approximation (LDA) and general gradient approximation (GGA) functionals. We used $18 \times 18 \times 18$ kmesh for all DFT calculations. We further used a combination of DFT (spin polarized version of LDA) and dynamical mean-field theory (DMFT) with spin-polarized T-matrix fluctuation impurity solver as implemented in RSPt code to correctly capture the correlation of Mn-3d orbitals for describing electronic structure. We used a k-mesh of $12 \times 12 \times 12$ for LSDA+DMFT to reduce the computational cost. The convergence with k-mesh used for integrations in BZ has been carefully checked for both DFT and DMFT.

The Heisenberg Hamiltonian describing the magnetic system is given by

$$H = - \sum_{ij} \sum_{\{\alpha, \beta\}} e_i^\alpha J_{ij}^{\alpha\beta} e_j^\beta \quad (1)$$

where e_i^α (e_j^β) is the α (β) component of the unitary vector pointing along the direction of the spin located at the site i (j). Considering $J_{ij}^{\alpha\beta}$ as a $[3 \times 3]$ matrix, the isotropic (Heisenberg) part of the magnetic exchange interactions J_{ij} 's and anti-symmetric Dzyaloshinskii–Moriya interactions (DMIs) D_{ij} 's are defined by

$$\begin{aligned} J_{ij} &= (J_{ij}^{xx} + J_{ij}^{yy} + J_{ij}^{zz})/3, \\ D_{ij} &= |\vec{D}_{ij}| = \sqrt{(D_{ij}^x)^2 + (D_{ij}^y)^2 + (D_{ij}^z)^2}, \end{aligned} \quad (2)$$

where $|\vec{D}|$ is the magnitude of the DMI vector. Here we used the convention of positive J_{ij} 's as ferromagnetic (FM) and negative J_{ij} 's as antiferromagnetic (AFM).

For a given real material, the parameters in expression (2) can be extracted from magnetic force theorem based on linear-response theory. This is originally formulated for the case of isotropic Heisenberg interactions in the absence of spin-orbit coupling (SOC) [52, 53]. The theory is formulated for second order perturbation in the deviations of spins from equilibrium magnetic configuration. The approach has been extended to take into account relativistic effects to allow to compute the full interaction tensor for $J_{ij}^{\alpha\beta}$ [54–57].

Here we present a derivation of the formulae based on Green's functions formalism below. We begin by perturbing the spin system by deviating the initial moments (\vec{e}_0) on a small angle $\delta\vec{\varphi}$ (the site index is omitted at the moment):

$$\vec{e} = \vec{e}_0 + \delta\vec{e} + \delta^2\vec{e} = \vec{e}_0 + [\delta\vec{\varphi} \times \vec{e}_0] - \frac{1}{2}\vec{e}_0(\delta\vec{\varphi})^2$$

Then one can write the Hamiltonian Eq. (1) of the perturbed system in terms of series in the order of $\delta\vec{\varphi}$:

$$\hat{H}' = \hat{H}^{(0)} + \hat{H}^{(1)} + \hat{H}^{(2)}.$$

In the collinear limit, all spins point along the same direction, which we set parallel to Z axis. Then the tilting vectors have the following components:

$$\begin{aligned}\vec{\delta\varphi} &= (\delta\varphi^x; \delta\varphi^y; 0) \\ [\vec{\delta\varphi} \times \vec{e}_0] &= (\delta\varphi^y; -\delta\varphi^x; 0)\end{aligned}$$

Focusing on the energy contributions of the second order in $\vec{\delta\varphi}$ (i.e. $\hat{H}^{(2)}$), we obtain:

$$\begin{aligned}H^{(2)} &= - \sum_{i \neq j} \left(J_{ij}^{xx} \delta\varphi_i^y \delta\varphi_j^y + J_{ij}^{yy} \delta\varphi_i^x \delta\varphi_j^x - J_{ij}^{xy} \delta\varphi_i^y \delta\varphi_j^x \right. \\ &\quad \left. - J_{ij}^{yx} \delta\varphi_i^x \delta\varphi_j^y - \frac{1}{2} J_{ij}^{zz} ((\delta\varphi_i)^2 + (\delta\varphi_j)^2) \right)\end{aligned}$$

Then one can do the same perturbation for the electronic Hamiltonian (\mathcal{H}), which will become:

$$\hat{\mathcal{H}}' = \hat{U}^\dagger \hat{\mathcal{H}} \hat{U} = \hat{\mathcal{H}}^{(0)} + \hat{\mathcal{H}}^{(1)} + \hat{\mathcal{H}}^{(2)},$$

where $\hat{U} = \exp(i\vec{\delta\varphi}\hat{\sigma}/2)$ and $\hat{\sigma}$ is the vector of Pauli matrices. The corresponding terms proportional to $\vec{\delta\varphi}$ can be identified and mapped onto generalized Heisenberg model. The expressions for various components of $J_{ij}^{\alpha\beta}$ (Eq. (1)) are obtained as

$$\begin{aligned}J_{ij}^{xx} &= \frac{T}{4} \sum_p \text{Tr}_{L,m} [\hat{\mathcal{H}}_i, \hat{\sigma}^y] G_{ij}(i\omega_p) [\hat{\mathcal{H}}_j, \hat{\sigma}^y] G_{ji}(i\omega_p) \\ J_{ij}^{xy} &= -\frac{T}{4} \sum_p \text{Tr}_{L,m} [\hat{\mathcal{H}}_i, \hat{\sigma}^y] G_{ij}(i\omega_p) [\hat{\mathcal{H}}_j, \hat{\sigma}^x] G_{ji}(i\omega_p)\end{aligned}$$

and similar expressions are also for J_{ij}^{yy} and J_{ij}^{yx} . The summation is done over the Matsubara frequencies (ω_p) and the trace is over the orbital indices denoted by m . The other components J_{ij}^{xz} , J_{ij}^{zx} , J_{ij}^{yz} , J_{ij}^{zy} are not of the second order in the tilting angles. Thus, for $M \parallel z$, only D_z component (Eq. (2)) can be computed, while D_x and D_y are extracted from two additional calculations with the magnetization pointing along x and y , respectively. We have used the method described above to calculate the magnetic exchange interactions of YMn_6Sn_6 as implemented within RSPt code [1].

B. Berry curvature and topological invariant

The Chern numbers (topological invariants) and Berry curvatures are calculated using a formalism based on Ref. [8]. The Chern number of n 'th band over a two-dimensional torus T^2 is given by

$$c_n = \frac{1}{2\pi i} \int_{T^2} d^2k F_{12}(k), \quad (3)$$

where the Berry field (Berry curvature) strength $F_{12}(k)$ and Berry connection $A_\mu(k)$ ($\mu = 1, 2$) are given by

$$\begin{aligned}F_{12}(k) &= \partial_1 A_2(k) - \partial_2 A_1(k), \\ A_\mu(k) &= \langle n(k) | \partial_\mu | n(k) \rangle,\end{aligned} \quad (4)$$

with $|k\rangle$ being a normalized wave function of the n th Bloch band such that $H(k)|k\rangle = E_n(k)|k\rangle$.

Now we consider a two-dimensional Brillouin zone (BZ) where $\mu = 1, 2$ could be x, y, z consisting of discrete lattice points k_ℓ given by ($\ell = 1, \dots, N_1 N_2$) given by

$$k_\ell = (k_{j_1}, k_{j_2}), \quad k_{j_\mu} = \frac{2\pi j_\mu}{q_\mu N_\mu}, \quad (j_\mu = 0, \dots, N_\mu - 1). \quad (5)$$

The Berry curvature is defined as

$$\begin{aligned}\tilde{F}_{12}(k_\ell) &\equiv \ln U_1(k_\ell) U_2(k_\ell + \hat{1}) U_1(k_\ell + \hat{2})^{-1} U_2(k_\ell)^{-1}, \\ -\pi &< \frac{1}{i} \tilde{F}_{12}(k_\ell) \leq \pi.\end{aligned} \quad (6)$$

where $U(1)$ is the scalar product of the wave function of the n th band at two consecutive reciprocal points in the BZ

$$U_\mu(k_\ell) \equiv \langle k_\ell | k_\ell + \hat{\mu} \rangle / \mathcal{N}_\mu(k_\ell), \quad (7)$$

with $\mathcal{N}_\mu(k_\ell) = |\langle k_\ell | k_\ell + \hat{\mu} \rangle|$. Finally, a new Chern number for n th band is calculated by summing up the imaginary part of the Berry curvature for the discrete points on the BZ and it is defined as

$$\tilde{c}_n \equiv \frac{1}{2\pi i} \sum_\ell \tilde{F}_{12}(k_\ell). \quad (8)$$

We used $400 \times 400 \times 1$ kmesh to calculate the Chern numbers and Berry curvature for YMn_6Sn_6 using the above formalism.

II. CRYSTAL STRUCTURE OF YMn_6Sn_6

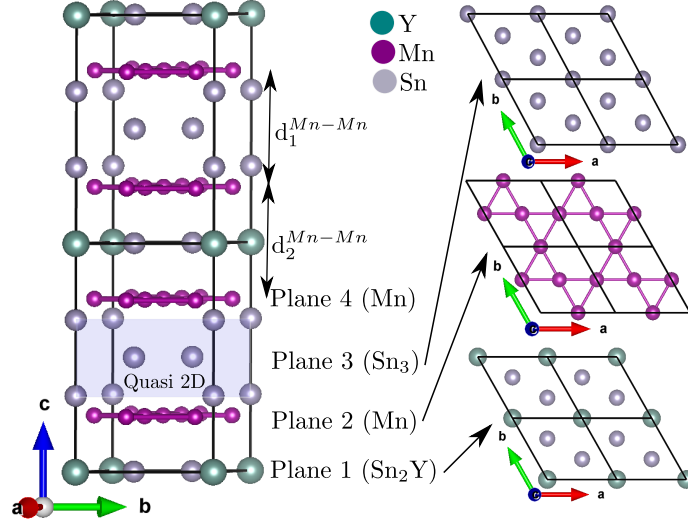


FIG. 5. Crystal structure of YMn_6Sn_6 . The black box corresponds to a single unit cell having four different planes [Sn_2Y , Mn, quasi 2D Sn_3 , Mn] including two different types of Mn kagome planes (plane 2 and plane 4).

We used the experimentally determined structure [10]. YMn_6Sn_6 crystallizes in a centrosymmetric layered structure with space group $P6/mmm$ (No. 191). The lattice parameters are $a = b = 5.536 \text{ \AA}$ and $c = 9.019 \text{ \AA}$. The structure consists of three two-dimensional (2D) planes and one quasi-2D structure, stacked along the c -axis as shown in Fig. 5. Of the three 2D planes, two are kagome planes made up of Mn atoms (called plane 2 and 4 in the following). The third 2D plane is a triangular lattice made up of Sn and Y atoms (called plane 1 in the following). The quasi-2D structure (called plane 3 in the following) consists of Sn atoms, and has a triangular structure in the ab -plane. The Mn-planes are spaced by the other two plane types in an alternating fashion. This means that the Mn planes are spaced with two different distances, $d_1^{\text{Mn}-\text{Mn}}$ and $d_2^{\text{Mn}-\text{Mn}}$ along the c -axis, with $d_1^{\text{Mn}-\text{Mn}} = 4.536 \text{ \AA}$ and $d_2^{\text{Mn}-\text{Mn}} = 4.483 \text{ \AA}$. The shorter distance is when the spacer layer is plane type 1, whereas plane type 3 is responsible for the slightly longer distance between the Mn planes. The in-plane Mn – Mn distance is 2.768 \AA . The space group for this type of magnetic kagome crystal structure has 24 point group symmetries, including the C_2 , C_3 , C_6 and inversion (P) symmetries.

III. MAGNETIC INTERACTIONS IN YMn_6Sn_6

To describe the exchange interactions properly, we used $1 \times 1 \times 2$ supercell of YMn_6Sn_6 (see Fig. 5), where the Mn – Mn across Sn_2Y and Sn_3 layers have AFM and FM interactions respectively. The calculated magnetic moment using different functionals are presented in the table I. The magnetic exchanges in YMn_6Sn_6 can be categorized into two parts : one is in-plane magnetic exchanges within a kagome plane (J_{ip} with $i = 1, 2, 3$) and other is magnetic exchanges along the c -axis (J_{ic} with $i = 1, 2, 3, 4, 5$) as shown in 6(a)-(b). The calculated J_{ic} 's ($i = 1, 2, 3, 4, 5$) for YMn_6Sn_6 from DFT, DFT with a Hubbard U and DFT+DMFT with a Hubbard $U = 2$ and 3 eV respectively are presented in a table II.

Computational method	magnetic moment (μ_B)
DFT	2.36
DFT+U (U=1 eV)	2.34
DFT+U (U=2 eV)	2.26
DFT+U (U=2.5 eV)	2.23
DFT+U (U=3 eV)	2.21
DFT+U (U=4 eV)	2.01
DFT+DMFT+U (U=2 eV)	2.29
DFT+DMFT+U (U=2.5 eV)	2.26
DFT+DMFT+U (U=3 eV)	2.23

TABLE I. Magnetic moment of YMn_6Sn_6 calculated from DFT and DFT+DMFT with inclusion of Hubbard U within LSDA.

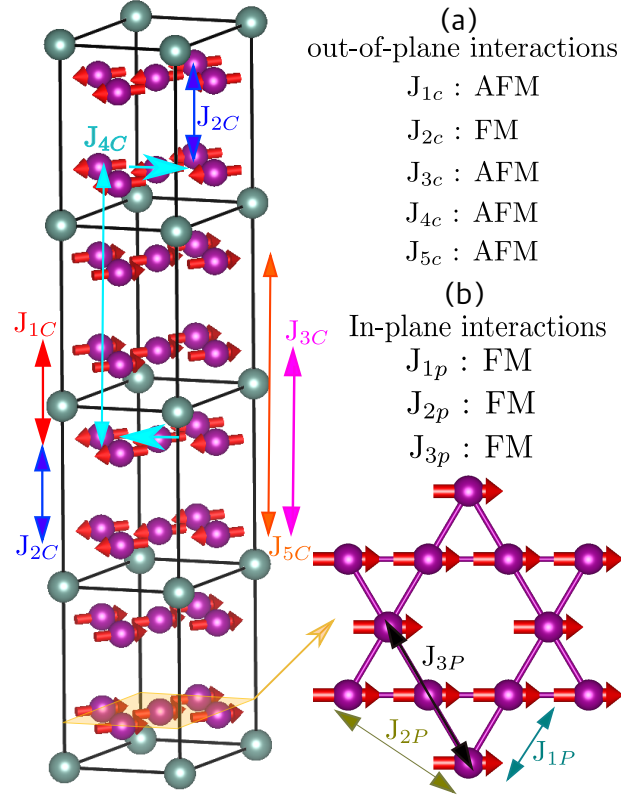


FIG. 6. The nearest neighbour magnetic exchange mapping in YMn_6Sn_6 for (a) out of plane (c -axis) and (b) in-plane (ab -plane) directions.

IV. SPIN TEXTURE OF YMn_6Sn_6

A. Spin texture from spin dynamics simulation

Table II shows pitch angle ϕ and the angle between two spirals from spin dynamics simulation (described in the main text) using full magnetic interactions parameters calculated with LSDA, LSDA+U and LSDA+DMFT with Hubbard $U = 2, 3$ eV respectively. We got magnetic ground state as a combination of two incommensurate spin spirals with

Method (ϕ, δ from spin dynamics simulation)	J_{1c} (AFM)	J_{2c} (FM)	J_{3c} (AFM)	J_{4c} (AFM)	J_{5c} (AFM)
DFT ($\phi = 0, \delta = 0$)	-11.74 meV	8.66 meV	-1.61 meV	-0.37 meV	-1.23 meV
DFT+U=2 ($\phi = 54^\circ, \delta = (1-10)^\circ$)	-8.01 meV	7.09 meV	-1.21 meV	-0.49 meV	-1.07 meV
DFT+U=3 ($\phi = 102^\circ, \delta = (3-11)^\circ$)	-4.51 meV	3.01 meV	-0.66 meV	-0.33 meV	-0.45 meV
DFT+DMFT+U=2 ($\phi = 58^\circ, \delta = 1.62^\circ$)	-11.13 meV	7.81 meV	-1.49 meV	-0.69 meV	-1.22 meV
DFT+DMFT+U=3 ($\phi = 89.3^\circ, \delta = 8.9^\circ$)	-9.17 meV	8.61 meV	-1.18 meV	-0.02 meV	-0.65 meV
Method (ϕ, δ from effective model)	J_{1c}^{eff} (FM)	J_{2c}^{eff} (FM)	J_{3c}^{eff} (FM/AFM)	J_{4c}^{eff} (FM/AFM)	J_{5c}^{eff} (AFM)
DFT ($\phi = 0, \delta = 0$)	1.12 meV	18.11 meV	0.702 meV (FM)	0.21 meV (FM)	-1.63 meV
DFT+DMFT+U=1 ($\phi = 0, \delta = 0$)	1.38 meV	15.26 meV	0.45 meV (FM)	-0.08 meV (AFM)	-1.32 meV
DFT+DMFT+U=2 ($\phi = 58.15^\circ, \delta = 9.1^\circ$)	2.49 meV	15.39 meV	0.13 meV (FM)	-0.54 meV (AFM)	-1.16 meV
DFT+DMFT+U=2.5 ($\phi = 77.7^\circ, \delta = 16.2^\circ$)	3.99 meV	16.44 meV	-0.34 meV (AFM)	-0.89 meV (AFM)	-1.67 meV
DFT+DMFT+U=3 ($\phi = 91.07^\circ, \delta = 14.77^\circ$)	4.08 meV	16.57 meV	-1.32 meV (AFM)	-1.62 meV (AFM)	-0.64 meV
DFT+DMFT+U=3.5 ($\phi = 0, \delta = 0$)	4.11 meV	17.12 meV	0.31 meV (FM)	0.61 meV (FM)	-0.73 meV
DFT+DMFT+U=4 ($\phi = 0, \delta = 0$)	4.68 meV	18.38 meV	1.21 meV (FM)	0.65 meV (FM)	-0.71 meV
DFT+U=1 ($\phi = 0, \delta = 0$)	1.50 meV	16.66 meV	0.55 meV (FM)	-0.06 meV (AFM)	-1.59 meV
DFT+U=2 ($\phi = 57.56^\circ, \delta = 8.38^\circ$)	1.48 meV	16.01 meV	0.43 meV (FM)	-0.22 meV (AFM)	-1.56 meV
DFT+U=2.5 ($\phi = 95.27^\circ, \delta = 11.01^\circ$)	1.37 meV	15.76 meV	0.15 meV (FM)	-0.68 meV (AFM)	-1.72 meV
DFT+U=3 ($\phi = 108.85^\circ, \delta = 10.69^\circ$)	1.79 meV	12.71 meV	-0.56 meV (AFM)	-0.78 meV (AFM)	-0.95 meV
DFT+U=3.5 ($\phi = 0, \delta = 0$)	1.37 meV	13.42 meV	0.17 meV (FM)	0.67 meV (FM)	-0.89 meV

TABLE II. Magnetic exchange interactions along the c -axis (J_{ic} with $i = 1, 2, 3, 4, 5$) and effective magnetic interactions within Mn planes along the c -axis (J_{ic}^{eff} with $i = 1, 2, 3, 4, 5$) calculated from DFT and DFT+DMFT with inclusion of Hubbard U within LSDA using $1 \times 1 \times 2$ supercell of YMn_6Sn_6 . The effective model is taken from Hamiltonian 9 in Sec. IV(B) to calculate ϕ, δ for second case which agreed well with our simulated results. Here we used the convention of positive (negative) J_{ij} 's as FM (AFM) respectively throughout the text.

a pitch angle ϕ of 54° (102°) originating from two different Mn kagome planes of YMn_6Sn_6 from LSDA+U with Hubbard U = 2 (3) eV respectively. The angle between two incommensurate spin spirals δ is also varying from $(1-10)^\circ$ ($(3-11)^\circ$) from LSDA+U with Hubbard U = 2 (3) eV respectively. We got the $\phi = 58^\circ$ (89.3°) and $\delta = 1.62^\circ$ (8.9°) from LSDA+DMFT with Hubbard U = 2 (3) eV respectively. We compare spin spiral wave vector q , pitch angle ϕ and angle between two incommensurate spin spirals δ of our magnetic ground state calculated from DFT+DMFT with a Hubbard U = 2, 3 eV with other experimental reports at low temperatures which are presented in the table III. Simulated ϕ and δ from LSDA+DMFT with Hubbard U = 3 eV matches well with experiment as shown in table III. The magnetic exchange interactions and spin spiral in YMn_6Sn_6 are very sensitive to structural parameters, temperatures and magnetic fields.

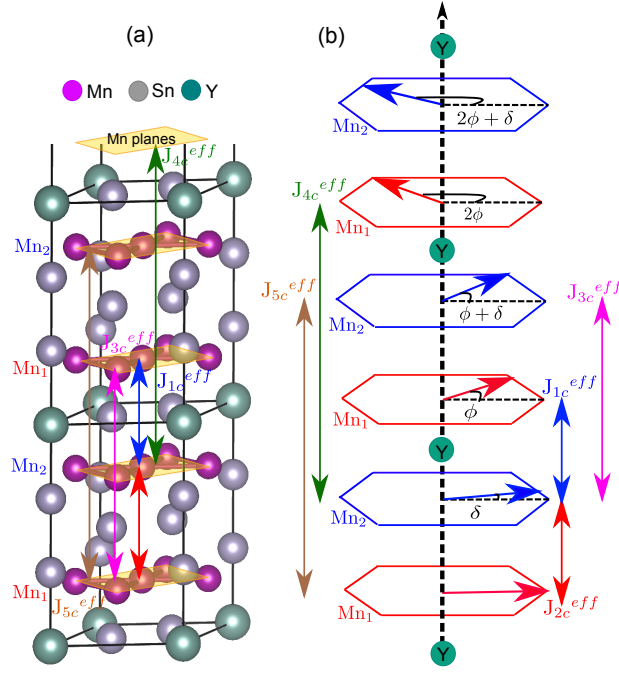


FIG. 7. (a) Effective magnetic interactions within Mn planes along the c -axis (J_{ic}^{eff} with $i=1,2,3,4,5$) in YMn_6Sn_6 . (b) Effective model of two spin spirals with five effective magnetic exchanges along c -axis J_{ic}^{eff} with $i=1,2,3,4,5$. Here ϕ is the pitch angle for both spirals and δ is the angle between two spin spirals.

B. Effective magnetic Hamiltonian for spin spiral of YMn_6Sn_6

We consider an effective Hamiltonian to describe the two incommensurate spin spirals in YMn_6Sn_6 given by :

$$\begin{aligned} H_{ic}^{eff} = & -J_{1c}^{eff} \cos(\phi - \delta) - J_{2c}^{eff} \cos \delta - 2J_{3c}^{eff} \cos \phi \\ & - J_{4c}^{eff} \cos(2\phi - \delta) - J_{5c}^{eff} \cos(\phi + \delta) \end{aligned} \quad (9)$$

where H_{ic}^{eff} is the effective model for two spin spiral with 5 magnetic effective magnetic exchanges along c -axis (J_{ic}^{eff} for $i=1,2,3,4,5$) extended from Rosenfeld et al. model with 3 magnetic effective magnetic exchanges along c -axis [14] (see Fig.7). Here ϕ is the pitch angle for both spirals and δ is the angle between two spin spirals. The effective magnetic exchanges J_{ic}^{eff} are calculated by summing over all out of plane magnetic exchanges within a plane. For example : $J_{1c}^{eff} = (J_2 + 4 \times J_5 + 4 \times J_8)$, $J_{2c}^{eff} = (J_3 + 4 \times J_6 + 4 \times J_9)$ and so on as shown in Fig.1(b) in the main text and Fig.7 (a). The effective magnetic exchange interactions J_{ic}^{eff} for $i=1,2,3,4,5$ calculated from different methods are shown in table II. The calculated ϕ and δ using effective magnetic exchanges between Mn planes along c -axis (J_{ic}^{eff} for $i=1,2,3,4,5$) are presented in table II for three different methods like LSDA, LSDA+U (with $U = 1, 2, 2.5, 3, 3.5$ eV) and LSDA+DMFT with a Hubbard $U = 1, 2, 2.5, 3, 3.5, 4$ eV. YMn_6Sn_6 gives a spin spiral phase with Hubbard $U = (2-3)$ eV and remains in FM phase for others U values from both LSDA+U and LSDA+DMFT with U as shown in table II. The calculated values are matches well with simulated spin spirals within UppASD [42] for three different methods presented in table II.

Figure 8 and 9 represents the energy evolution of pitch angle with calculated δ and $\delta = 0$ from both LSDA+U and LSDA+DMFT with Hubbard $U = 2, 2.5, 3$ eV respectively using the effective Hamiltonian 9 (see also table II). The energy differences between calculated and experimental (pitch angle $\phi \sim 90^\circ$) spin spirals are 0.355 meV, 0.11 and 0 meV from LSDA+DMFT with $U = 2, 2.5, 3$ respectively, whereas the corresponding energy difference is 0.185 meV, 0.015, 0.203 meV from LSDA+U with $U = 2, 2.5, 3$ eV respectively. The calculated pitch angle $\phi = 91.07^\circ$ for the spin spiral matches with the experimental value from LSDA+DMFT with $U = 3$ eV ($\Delta E_{Cal-Exp} = 0$), whereas calculated $\phi = 95.27^\circ$ for the spin spiral close to the experimental value from LSDA+U with $U = 2.5$ eV ($\Delta E_{Cal-Exp} = 0.015$ meV). Putting $\delta = 0$ i.e angle between two non-equivalent, incommensurate spin spirals zero, the asymmetric double well nature of the energy evolution transforms into symmetric double well which indicates the two equivalent, incommensurate spin spirals in YMn_6Sn_6 (see Fig.8 and Fig.9).

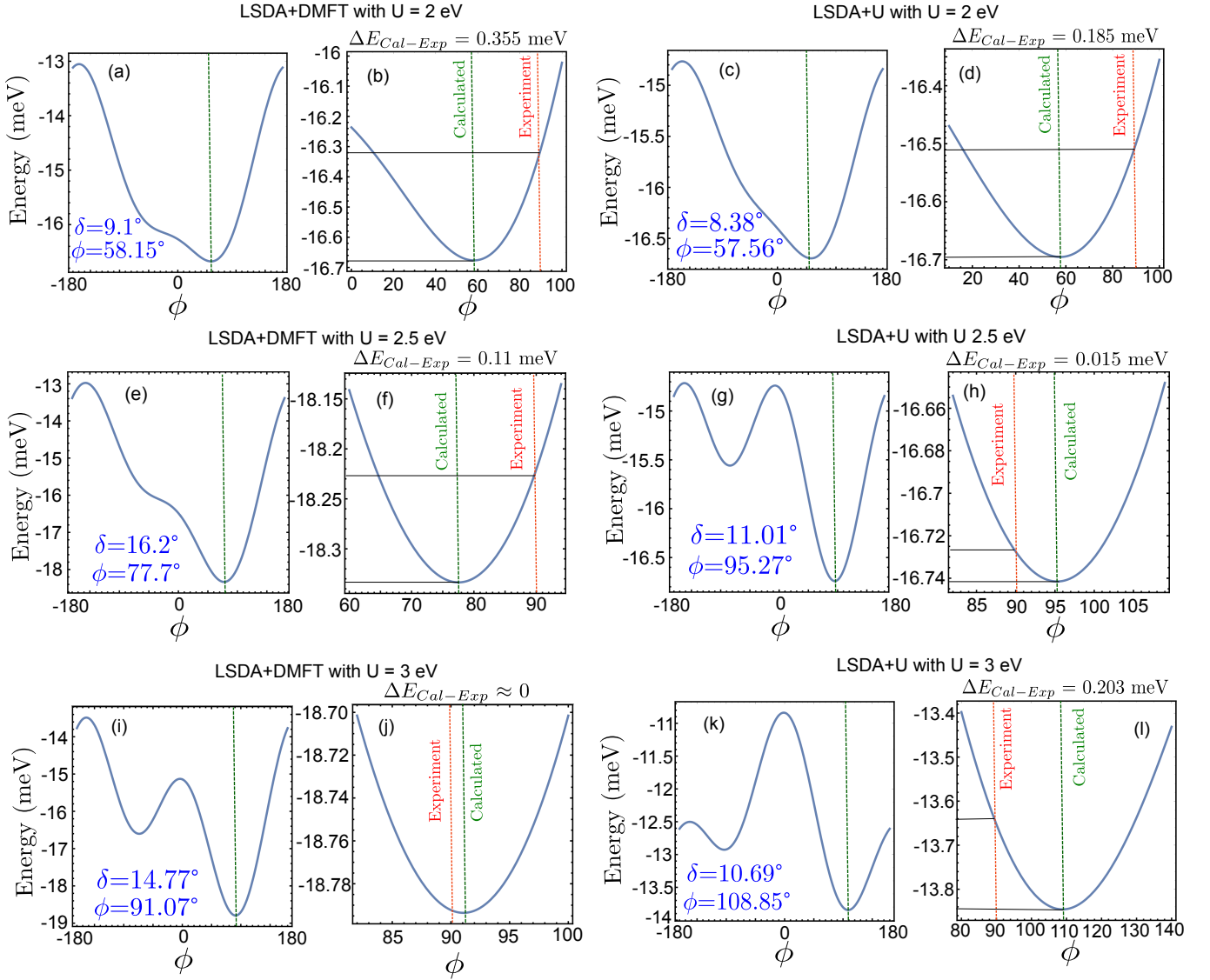


FIG. 8. Calculated variation of energy with the pitch angle from (a)-(b) LSDA+DMFT and (c)-(d) LSDA+U with $U = 2$ eV, (e)-(f) LSDA+DMFT and (g)-(h) LSDA+U with $U = 2.5$ eV, (i)-(j) LSDA+DMFT and (k)-(l) LSDA+U with $U = 3$ eV using the model Hamiltonian in 9 (Sec. IV(B)) with calculated δ . The calculated pitch angles are compared with experimental report [12].

V. MAGNON BAND STRUCTURES OF $Y\text{Mn}_6\text{Sn}_6$

Figure 10(a) shows magnon band structure of $Y\text{Mn}_6\text{Sn}_6$ without SOC from LSDA+DMFT with $U = 2$ eV. Here the calculated magnetic exchanges within a kagome plane are $J_{1p} = 9.52$ meV, $J_{2p} = 0.76$ meV respectively and out of plane magnetic exchanges are $J_{1c} = -7.16$ meV, $J_{2c} = 4.52$ meV respectively. The Dirac band crossing (Dirac magnon) appears at 73 meV at high symmetry K point which is in good agreement with experimental report [10]. To compare with calculated magnon spectra with the experimental study reported by Zhang et al. [10], we calculated the dynamical structure factor $S(\mathbf{q}, \omega)$ from spin dynamics simulation at $T = 5$. This is in good agreement with the experimental measured spectra with LSDA+DMFT with $U = 2$ eV as shown in 10(a). Furthermore, we compared the lowest magnon band along the path $\Gamma_1(2\ 0\ 0) - K_4(5/3\ -1/3\ 0) - M_5(2\ -1/2\ 0) - \Gamma_1(2\ 0\ 0)$ [10] which is excellent agreement with the experimental observation as shown in Fig.10(b). Another Dirac crossing appears at 100 meV. Both the Dirac crossings open topological gap with inclusion of SOC at that point.

We calculated the magnon bands for quasi 2D kagome plane of $Y\text{Mn}_6\text{Sn}_6$ (as shown in Fig.11(a) where J_{ij} 's and D_{ij} 's are taken from bulk calculations) to study the effect of in-plane magnetic (ab -plane) interactions on magnon topology. Figure 11(b) represents the magnon bands from LSDA+DMFT with $U = 3$ eV with SOC. Here the in-plane

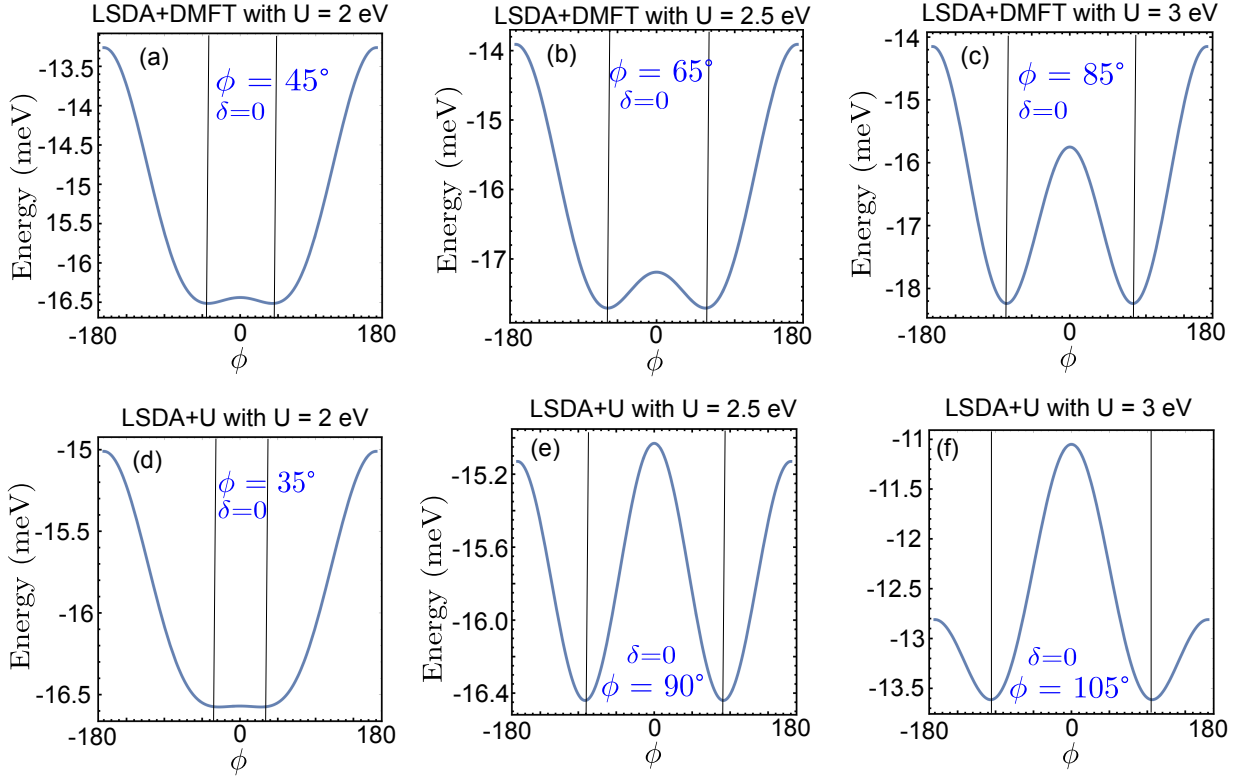


FIG. 9. Calculated variation of energy with the pitch angle from (a) LSDA+DMFT with $U = 2$ eV and (b) LSDA+U with $U = 2$ eV, (c) LSDA+U with $U = 3$ eV using the model Hamiltonian in 9 (Sec. IV) with $\delta=0$.

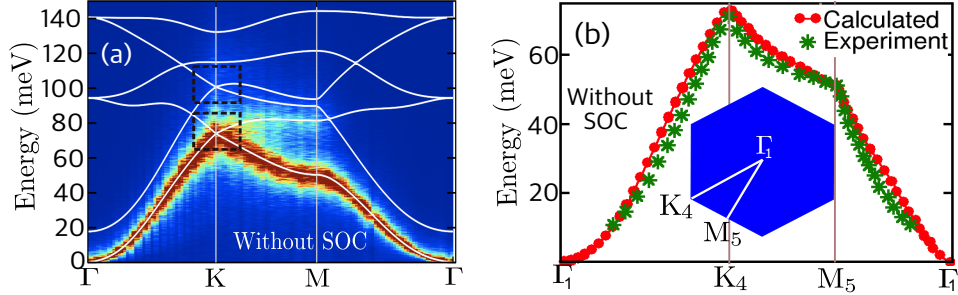


FIG. 10. (a) Magnon bands in YMn_6Sn_6 without SOC along (a) $\Gamma(0\ 0\ 0) - \text{K}(1/3\ 1/3\ 0) - \text{M}(1/2\ 0\ 0) - \Gamma(0\ 0\ 0)$ and (b) $\Gamma_1(2\ 0\ 0) - \text{K}_4(5/3\ -1/3\ 0) - \text{M}_5(2\ -1/2\ 0) - \Gamma_1(2\ 0\ 0)$. The Dirac points are marked by boxes in the left figure and the lowest magnon band is in good agreement with the observed magnon spectra according to the experimental report by Zhang et.al. [10].

magnetic exchange $J_{1p} \sim 4.85$ meV. The in-plane and out of plane components of DMIs are $D_{1p}^{\parallel} \sim 0.218$ meV and $D_{1p}^z \sim 0$ respectively. We got a gapless mode if include only the first nearest neighbour magnetic interactions as $\frac{D_{1p}^z}{J_{1p}} \sim 0$. However, this opens a gap of ~ 0.6 meV at high symmetry K point around ~ 62 meV with inclusion of $D_{2p}^z \sim 0.308$ meV as shown in Fig.11(b). The Chern numbers of upper, middle and lower magnon bands are $c = -1, 0, 1$ respectively. Flat bands with nonzero Chern number ($c = -1$) (see Fig.11(b)) and Berry curvature profile (see Fig.11(c)) ensure the landmark of topological magnon in incommensurate spin spiral of YMn_6Sn_6 .

VI. ELECTRONIC BAND STRUCTURES OF YMn_6Sn_6

We calculated the electronic band structure of YMn_6Sn_6 from LDA+DMFT with a Hubbard $U = 2, 3$ eV and a Hund's coupling $J = 0.7$ eV. Figure 12(a)-(b) show the band structures of YMn_6Sn_6 without and with SOC along the high symmetry $M - \Gamma - M - K - \Gamma - K - A - \Gamma - A$ directions in the hexagonal Brillouin zone (BZ) with a Hubbard

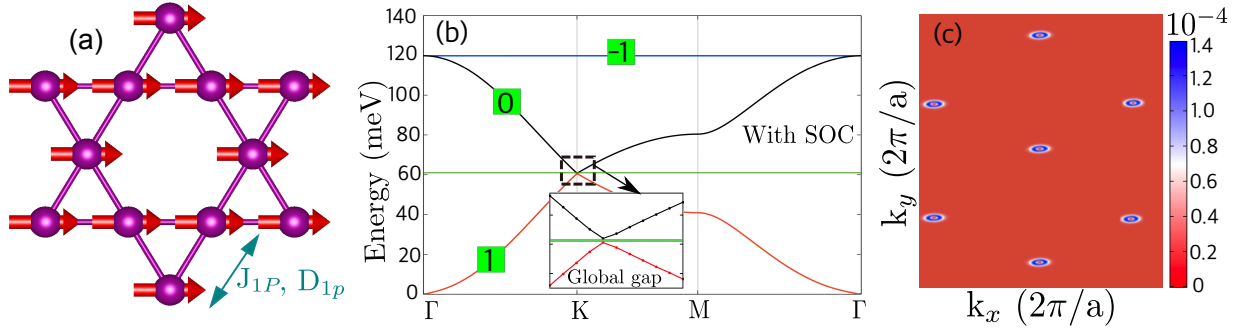


FIG. 11. (a) Mn Kagome plane, (b) magnon bands and (c) Berry curvature profile for quasi 2D structure of YMn_6Sn_6 .

$U = 2$ eV and a Hund's coupling $J = 0.7$ eV on Mn $-3d$ orbitals. Two Dirac points (DPs) DP_1 and DP_2 are located at about $\sim 0.038, 0.279$ eV below and above the Fermi level E_f at the high symmetry K point respectively which are in good agreement with experimental report where DPs appeared at $\sim 0.04, 0.3$ eV respectively [58]. With inclusion of SOC, gaps open at high symmetry K point around the DPs. Another feature is the observation of flat band at about ~ 0.4 eV below E_f which exists throughout the whole BZ [58]. The flat bands are pushed to E_f with further increasing Hubbard interaction to $U = 3$ eV as shown in Fig. 12(c).

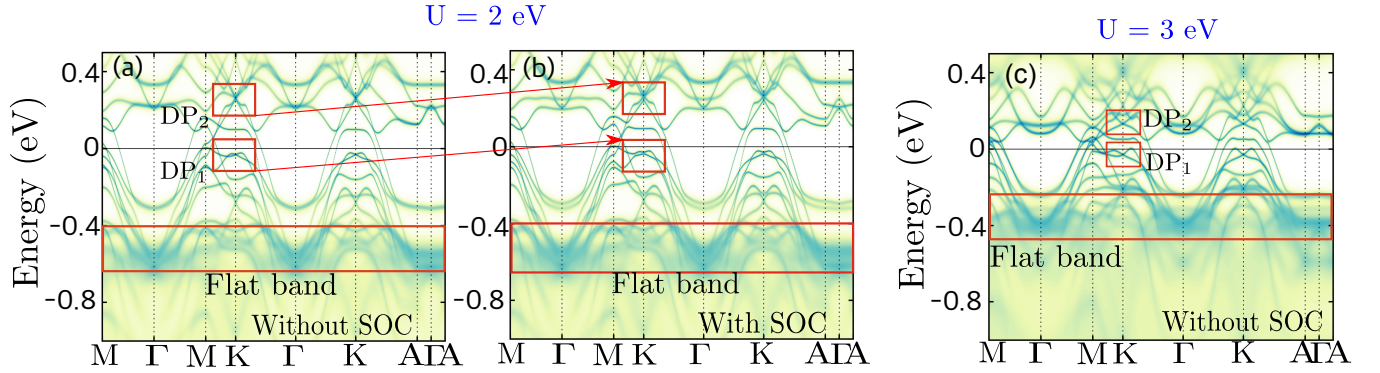


FIG. 12. Band structures from LDA+DMFT with (a)-(b) $U=2$ eV without and with SOC respectively, and (c) $U=3$ eV without SOC where the Dirac points are marked by boxes.

-
- [1] Full-Potential Electronic Structure Method: energy and force calculations with density functional and dynamical mean field theory, Wills, John M and Alouani, Mebarek and Andersson, Per and Delin, Anna and Eriksson, Olle and Grechnev, Oleksiy, *Springer Science & Business Media* (2010)
 - [2] Liechtenstein, A Il and Katsnelson, MI and Antropov, VP and Gubanov, VA, *Journal of Magnetism and Magnetic Materials* **67**, 65-74 (1987)
 - [3] Katsnelson. M.I and Liechtenstein A. I, *Phys. Rev. B* **61**, 8906 (2000)
 - [4] Antropov, VP and Katsnelson, MI and Liechtenstein, AI, *Physica B: Condensed Matter* **237**, 336-340 (1997)
 - [5] Udvardi, L. and Szunyogh, L. and Palotás, K. and Weinberger, P., *Phys. Rev. B* **68**, 104436 (2003)
 - [6] Ebert, H. and Mankovsky, S., *Phys. Rev. B* **79**, 045209 (2009)
 - [7] Secchi, Andrea and Lichtenstein, Alexander I and Katsnelson, Mikhail I, *Annals of Physics* **360**, 61-97 (2015)
 - [8] T. Fukui, Y. Hatsugai, and H. Suzuki, *Journal of the Physical Society of Japan* **74**, 1674 (2005)
 - [9] <http://github.com/UppASD/UppASD>
 - [10] H. Zhang, X. Feng, T. Heitmann, A. I. Kolesnikov, M. B. Stone, Y.-M. Lu, and X. Ke, *Phys. Rev. B* **101**, 100405 (2020)
 - [11] Li, Man and Wang, Qi and Wang, Guangwei and Yuan, Zhihong and Song, Wenhua and Lou, Rui and Liu, Zhengtai and Huang, Yaobo and Liu, Zhonghao and Lei, Hechang and Yin, Zhiping and Wang, Shancai *Nature Communications* **12**, 3129 (2021).
 - [12] N. J. Ghimire, R. L. Dally, L. Poudel, D. C. Jones, D. Michel, N. T. Magar, M. Bleuel, M. A. McGuire, J. S. Jiang, J. F. Mitchell, J. W. Lynn, and I. I. Mazin, *Sci. Adv.* **6**, eabe2680 (2020).
 - [13] C. Q. Xu, T. W. Heitmann, H. Zhang, Xiaofeng Xu, and X. Ke, *Phys. Rev. B* **104**, 024413 (2021).

- [14] E. Rosenfeld and N. Mushnikov, *Physica B* **403**, 1898 (2008).
- [15] Rebecca L. Dally, Jeffrey W. Lynn, Nirmal J. Ghimire, Dina Michel, Peter Siegfried, and Igor I. Mazin, *Phys. Rev. B* **103**, 094413 (2021).
- [16] Tian-Heng Han, Joel S. Helton, Shaoyan Chu, Daniel G. Nocera, Jose A. Rodriguez-Rivera, Collin Broholm, and Young S. Lee, “Fractionalized excitations in the spin-liquid state of a kagome-lattice antiferromagnet,” *Nature* **492**, 406–410 (2012).
- [17] Kenya Ohgushi, Shuichi Murakami, and Naoto Nagaosa, “Spin anisotropy and quantum hall effect in the kagomé lattice: Chiral spin state based on a ferromagnet,” *Phys. Rev. B* **62**, R6065–R6068 (2000).
- [18] Nirmal J. Ghimire and Igor I. Mazin, “Topology and correlations on the kagome lattice,” *Nature Materials* **19**, 137–138 (2020).
- [19] Yi Zhou, Kazushi Kanoda, and Tai-Kai Ng, “Quantum spin liquid states,” *Rev. Mod. Phys.* **89**, 025003 (2017).
- [20] Tian-Heng Han, Joel S. Helton, Shaoyan Chu, Daniel G. Nocera, Jose A. Rodriguez-Rivera, Collin Broholm, and Young S. Lee, “Fractionalized excitations in the spin-liquid state of a kagome-lattice antiferromagnet,” *Nature* **492**, 406–410 (2012).
- [21] Jia-Xin Yin, Songtian S. Zhang, Guoqing Chang, Qi Wang, Stepan S. Tsirkin, Zurab Guguchia, Biao Lian, Huibin Zhou, Kun Jiang, Ilya Belopolski, Nana Shumiya, Daniel Multer, Maksim Litskevich, Tyler A. Cochran, Hsin Lin, Ziqiang Wang, Titus Neupert, Shuang Jia, Hechang Lei, and M. Zahid Hasan, “Negative flat band magnetism in a spin–orbit-coupled correlated kagome magnet,” *Nature Physics* **15**, 443–448 (2019).
- [22] Enke Liu, Yan Sun, Nitesh Kumar, Lukas Muechler, Aili Sun, Lin Jiao, Shuo-Ying Yang, Defa Liu, Aiji Liang, Qiunan Xu, Johannes Kroder, Vicky Süß, Horst Borrmann, Chandra Shekhar, Zhaosheng Wang, Chuanying Xi, Wenhong Wang, Walter Schnelle, Steffen Wirth, Yulin Chen, Sebastian T. B. Goennenwein, and Claudia Felser, “Giant anomalous hall effect in a ferromagnetic kagome-lattice semimetal,” *Nature Physics* **14**, 1125–1131 (2018).
- [23] Mingu Kang, Linda Ye, Shiang Fang, Jhih-Shih You, Abe Levitan, Minyong Han, Jorge I. Facio, Chris Jozwiak, Aaron Bostwick, Eli Rotenberg, Mun K. Chan, Ross D. McDonald, David Graf, Konstantine Kaznatcheev, Elio Vescovo, David C. Bell, Efthimios Kaxiras, Jeroen van den Brink, Manuel Richter, Madhav Prasad Ghimire, Joseph G. Checkelsky, and Riccardo Comin, “Dirac fermions and flat bands in the ideal kagome metal fesn,” *Nature Materials* **19**, 163–169 (2020).
- [24] J-X Yin, Nana Shumiya, Sougata Mardanya, Qi Wang, Songtian S. Zhang, Hung-Ju Tien, Daniel Multer, Yuxiao Jiang, Guangming Cheng, Nan Yao, Shangfei Wu, Desheng Wu, Liangzi Deng, Zhipeng Ye, Rui He, Guoqing Chang, Zhonghao Liu, Kun Jiang, Ziqiang Wang, Titus Neupert, Amit Agarwal, Tay-Rong Chang, Ching-Wu Chu, Hechang Lei, and M. Zahid Hasan, “Fermion-boson many-body interplay in a frustrated kagome paramagnet,” *Nature Communications* **11**, 4003 (2020).
- [25] Yang Zhang, Yan Sun, Hao Yang, Jakub Železný, Stuart P. P. Parkin, Claudia Felser, and Binghai Yan, “Strong anisotropic anomalous hall effect and spin hall effect in the chiral antiferromagnetic compounds mn_3x ($x = \text{Ge}, \text{sn}, \text{ga}, \text{ir}, \text{rh}$, and pt),” *Phys. Rev. B* **95**, 075128 (2017).
- [26] Pyeongjae Park, Joosung Oh, Klára Uhlířová, Jerome Jackson, András Deák, László Szunyogh, Ki Hoon Lee, Hwanbeom Cho, Ha-Leem Kim, Helen C Walker, Devashibhai Adroja, Vladimír Sechovský, and Je-Geun Park, “Magnetic excitations in non-collinear antiferromagnetic weyl semimetal Mn_3Sn ,” *npj Quantum Materials* **3**, 63 (2018).
- [27] Yutaro Takeuchi, Yuta Yamane, Ju-Young Yoon, Ryuichi Itoh, Butsurin Jinnai, Shun Kanai, Jun’ichi Ieda, Shunsuke Fukami, and Hideo Ohno, “Chiral-spin rotation of non-collinear antiferromagnet by spin–orbit torque,” *Nature Materials* **20**, 1364–1370 (2021).
- [28] Dongwook Go, Moritz Sallermann, Fabian R. Lux, Stefan Blügel, Olena Gomonay, and Yuriy Mokrousov, “Non-collinear spin current for switching of chiral magnetic textures,” *arXiv preprint arXiv:2201.11476* (2022).
- [29] S. Sinnema, R.J. Radwanski, J.J.M. Franse, D.B. de Mooij, and K.H.J. Buschow, “Magnetic properties of ternary rare-earth compounds of the type $\text{r}_2\text{fe}_4\text{b}$,” *Journal of Magnetism and Magnetic Materials* **44**, 333–341 (1984).
- [30] M.S.S. Brooks, L. Nordström, and B. Johansson, “Rare-earth transition-metal intermetallics,” *Physica B: Condensed Matter* **172**, 95–100 (1991).
- [31] B. Malaman, G. Venturini, R. Welter, J.P. Sanchez, P. Vulliet, and E. Ressouche, “Magnetic properties of RMn_6Sn_6 ($\text{R}=\text{Gd}-\text{Er}$) compounds from neutron diffraction and mössbauer measurements,” *Journal of Magnetism and Magnetic Materials* **202**, 519–534 (1999).
- [32] D.M. Clatterbuck and K.A. Gschneidner, “Magnetic properties of RMn_6Sn_6 ($\text{R}=\text{Tb}, \text{Ho}, \text{Er}, \text{Tm}, \text{Lu}$) single crystals,” *Journal of Magnetism and Magnetic Materials* **207**, 78–94 (1999).
- [33] Jia-Xin Yin, Wenlong Ma, Tyler A. Cochran, Xitong Xu, Songtian S. Zhang, Hung-Ju Tien, Nana Shumiya, Guangming Cheng, Kun Jiang, Biao Lian, Zhida Song, Guoqing Chang, Ilya Belopolski, Daniel Multer, Maksim Litskevich, Zi-Jia Cheng, Xian P. Yang, Bianca Swidler, Huibin Zhou, Hsin Lin, Titus Neupert, Ziqiang Wang, Nan Yao, Tay-Rong Chang, Shuang Jia, and M. Zahid Hasan, “Quantum-limit chern topological magnetism in TbMn_6Sn_6 ,” *Nature* **583**, 533–536 (2020).
- [34] Wenlong Ma, Xitong Xu, Zihe Wang, Huibin Zhou, Madalynn Marshall, Zhe Qu, Weiwei Xie, and Shuang Jia, “Anomalous hall effect in the distorted kagome magnets $(\text{Nd}, \text{Sm})\text{Mn}_6\text{Sn}_6$,” *Phys. Rev. B* **103**, 235109 (2021).
- [35] Rebecca L. Dally, Jeffrey W. Lynn, Nirmal J. Ghimire, Dina Michel, Peter Siegfried, and Igor I. Mazin, “Chiral properties of the zero-field spiral state and field-induced magnetic phases of the itinerant kagome metal YMn_6Sn_6 ,” *Phys. Rev. B* **103**, 094413 (2021).
- [36] Qi Wang, Kelly J. Neubauer, Chunruo Duan, Qiangwei Yin, Satoru Fujitsu, Hideo Hosono, Feng Ye, Rui Zhang, Songxue Chi, Kathryn Krycka, Hechang Lei, and Pengcheng Dai, “Field-induced topological hall effect and double-fan spin structure with a c -axis component in the metallic kagome antiferromagnetic compound YMn_6Sn_6 ,” *Phys. Rev. B* **103**, 014416 (2021).
- [37] Nirmal J. Ghimire, Rebecca L. Dally, L. Poudel, D. C. Jones, D. Michel, N. Thapa Magar, M. Bleuel, Michael A. McGuire, J. S. Jiang, J. F. Mitchell, Jeffrey W. Lynn, and I. I. Mazin, “Competing magnetic phases and

- fluctuation-driven scalar spin chirality in the kagome metal YMn_6Sn_6 ,” *Science Advances* **6**, eabe2680 (2020), <https://www.science.org/doi/pdf/10.1126/sciadv.abe2680>.
- [38] EV Rosenfeld and NV Mushnikov, “Double-flat-spiral magnetic structures: Theory and application to the RMn_6X_6 compounds,” *Physica B: Condensed Matter* **403**, 1898–1906 (2008).
- [39] H. Zhang, X. Feng, T. Heitmann, A. I. Kolesnikov, M. B. Stone, Y.-M. Lu, and X. Ke, “Topological magnon bands in a room-temperature kagome magnet,” *Phys. Rev. B* **101**, 100405 (2020).
- [40] C. Q. Xu, T. W. Heitmann, H. Zhang, Xiaofeng Xu, and X. Ke, “Magnetic phase transition, magnetoresistance, and anomalous hall effect in Ga-substituted YMn_6X_6 with a ferromagnetic kagome lattice,” *Phys. Rev. B* **104**, 024413 (2021).
- [41] See supplemental materials xxxx-xxxx for the discussion on the following sections : “Theoretical and computational details”; and “Crystal structure of YMn_6Sn_6 ”; and “Magnetic interactions”; and “Spin textures from both spin dynamics simulationa and effective model Hamiltonian”; and “Magnon band structure”; and “Electronic band structure” of YMn_6Sn_6 ”.
- [42] [Http://github.com/UppASD/UppASD](http://github.com/UppASD/UppASD).
- [43] David C. Johnston, “Magnetic structure and magnetization of helical antiferromagnets in high magnetic fields perpendicular to the helix axis at zero temperature,” *Phys. Rev. B* **96**, 104405 (2017).
- [44] K. Matan, D. Grohol, D. G. Nocera, T. Yildirim, A. B. Harris, S. H. Lee, S. E. Nagler, and Y. S. Lee, “Spin waves in the frustrated kagomé lattice antiferromagnet $\text{kFe}_3(\text{OH})_6(\text{SO}_4)_2$,” *Phys. Rev. Lett.* **96**, 247201 (2006).
- [45] R. Chisnell, J. S. Helton, D. E. Freedman, D. K. Singh, R. I. Bewley, D. G. Nocera, and Y. S. Lee, “Topological magnon bands in a kagome lattice ferromagnet,” *Phys. Rev. Lett.* **115**, 147201 (2015).
- [46] Sebastián A. Díaz, Jelena Klinovaja, and Daniel Loss, “Topological magnons and edge states in antiferromagnetic skyrmion crystals,” *Phys. Rev. Lett.* **122**, 187203 (2019).
- [47] Wanxiang Feng, Di Xiao, Jun Ding, and Yugui Yao, “Three-dimensional topological insulators in I–III– vi_2 and II–IV– v_2 chalcopyrite semiconductors,” *Phys. Rev. Lett.* **106**, 016402 (2011).
- [48] Surasree Sadhukhan, Banasree Sadhukhan, and Sudipta Kanungo, “Pressure-driven tunable properties of the small-gap chalcopyrite topological quantum material zngesb_2 : A first-principles study,” *Phys. Rev. B* **106**, 125112 (2022).
- [49] Maximilian Trescher and Emil J. Bergholtz, “Flat bands with higher chern number in pyrochlore slabs,” *Phys. Rev. B* **86**, 241111 (2012).
- [50] Banasree Sadhukhan and Tanay Nag, “Effect of chirality imbalance on hall transport of prrh_2 ,” *Phys. Rev. B* **107**, L081110 (2023).
- [51] Alexander Mook, Jürgen Henk, and Ingrid Mertig, “Magnon hall effect and topology in kagome lattices: A theoretical investigation,” *Phys. Rev. B* **89**, 134409 (2014).
- [52] A Il Liechtenstein, MI Katsnelson, VP Antropov, and VA Gubanov, “Local spin density functional approach to the theory of exchange interactions in ferromagnetic metals and alloys,” *Journal of Magnetism and Magnetic Materials* **67**, 65–74 (1987).
- [53] M. I. Katsnelson and A. I. Lichtenstein, “First-principles calculations of magnetic interactions in correlated systems,” *Phys. Rev. B* **61**, 8906–8912 (2000).
- [54] VP Antropov, MI Katsnelson, and AI Liechtenstein, “Exchange interactions in magnets,” *Physica B: Condensed Matter* **237**, 336–340 (1997).
- [55] L. Udvardi, L. Szunyogh, K. Palotás, and P. Weinberger, “First-principles relativistic study of spin waves in thin magnetic films,” *Phys. Rev. B* **68**, 104436 (2003).
- [56] H. Ebert and S. Mankovsky, “Anisotropic exchange coupling in diluted magnetic semiconductors: Ab initio spin-density functional theory,” *Phys. Rev. B* **79**, 045209 (2009).
- [57] Andrea Secchi, Alexander I Lichtenstein, and Mikhail I Katsnelson, “Magnetic interactions in strongly correlated systems: Spin and orbital contributions,” *Annals of Physics* **360**, 61–97 (2015).
- [58] Man Li, Qi Wang, Guangwei Wang, Zhihong Yuan, Wenhua Song, Rui Lou, Zhengtai Liu, Yaobo Huang, Zhonghao Liu, Hechang Lei, Zhiping Yin, and Shancai Wang, “Dirac cone, flat band and saddle point in kagome magnet YMn_6Sn_6 ,” *Nature Communications* **12**, 3129 (2021)

Experimental report	spin spiral wave vector	pitch angle ϕ	angle between two spirals δ
Ghimire et al. [12] $d_{[\text{Sn}_2\text{Y}]} > d_{[\text{Sn}_3]}$ $J_{1c} (J_{[\text{Sn}_3]}) : \text{FM}, J_{2c} (J_{[\text{Sn}_2\text{Y}]}) : \text{AFM}, J_{3c} : \text{FM}$	0.25	90°	20°
Xu et al. [13] $d_{[\text{Sn}_2\text{Y}]} > d_{[\text{Sn}_3]}$ $J_{1c} (J_{[\text{Sn}_3]}) : \text{FM}, J_{2c} (J_{[\text{Sn}_2\text{Y}]}) : \text{FM}, J_{3c} : \text{AFM}$	0.266	95.6°	-
Rosenfeld et al. [14] $d_{[\text{Sn}_2\text{Y}]} > d_{[\text{Sn}_3]}$ $J_{1c} (J_{[\text{Sn}_3]}) : \text{FM}, J_{2c} (J_{[\text{Sn}_2\text{Y}]}) : \text{FM}, J_{3c} : \text{AFM}$	$q_1 = 0.2796$ and $q_2 = 0.2545$	101°	11°
Zhang et al. [10] $d_{[\text{Sn}_2\text{Y}]} < d_{[\text{Sn}_3]}$ $J_{1c} (J_{[\text{Sn}_2\text{Y}]}) : \text{AFM}, J_{2c} (J_{[\text{Sn}_3]}) : \text{FM}, J_{3c} : -$	0.266	95.6°	-
Our study : simulation with $U = 2 \text{ eV}$ $d_{[\text{Sn}_2\text{Y}]} < d_{[\text{Sn}_3]}$ $J_{1c} (J_{[\text{Sn}_2\text{Y}]}) : \text{AFM}, J_{2c} (J_{[\text{Sn}_3]}) : \text{FM}, J_{3c} : \text{AFM}$	0.1615	$\sim 58^\circ (\pm 0.2)$	$\sim 1.62^\circ (\pm 0.01)$
Our study : simulation with $U = 3 \text{ eV}$ $d_{[\text{Sn}_2\text{Y}]} < d_{[\text{Sn}_3]}$ $J_{1c} (J_{[\text{Sn}_2\text{Y}]}) : \text{AFM}, J_{2c} (J_{[\text{Sn}_3]}) : \text{FM}, J_{3c} : \text{AFM}$	0.248	$\sim 89.5^\circ (\pm 0.5)$	$\sim 8.9^\circ (\pm 0.06)$
Our study : effective model from Sec. IV, $U = 2 \text{ eV}$ $d_{[\text{Sn}_2\text{Y}]} < d_{[\text{Sn}_3]}$ $J_{1c}^{eff} (J_{[\text{Sn}_2\text{Y}]}) : \text{FM}, J_{2c}^{eff} (J_{[\text{Sn}_3]}) : \text{FM}, J_{3c}^{eff} : \text{FM}$		$\sim 58.15^\circ$	$\sim 9.1^\circ$
Our study : effective model from Sec. IV, $U = 2.5 \text{ eV}$ $d_{[\text{Sn}_2\text{Y}]} < d_{[\text{Sn}_3]}$ $J_{1c}^{eff} (J_{[\text{Sn}_2\text{Y}]}) : \text{FM}, J_{2c}^{eff} (J_{[\text{Sn}_3]}) : \text{FM}, J_{3c}^{eff} : \text{AFM}$		$\sim 77.7^\circ$	$\sim 16.2^\circ$
Our study : effective model from Sec. IV, $U = 3 \text{ eV}$ $d_{[\text{Sn}_2\text{Y}]} < d_{[\text{Sn}_3]}$ $J_{1c}^{eff} (J_{[\text{Sn}_2\text{Y}]}) : \text{FM}, J_{2c}^{eff} (J_{[\text{Sn}_3]}) : \text{FM}, J_{3c}^{eff} : \text{AFM}$		$\sim 91.07^\circ$	$\sim 14.47^\circ$

TABLE III. Spin spiral wave vector q , pitch angle ϕ and angle between two spin spirals δ in YMn_6Sn_6 from different experimental studies at low temperatures. Magnetic exchange interactions and ground state are very much sensitive to structural parameters. $d_{[\text{Sn}_3]}$ and $d_{[\text{Sn}_2\text{Y}]}$ are the Mn – Mn layers distance separated by $[\text{Sn}_3]$ and $[\text{Sn}_2\text{Y}]$ layers respectively as described in Fig.5. $J_{[\text{Sn}_3]}$ and $J_{[\text{Sn}_2\text{Y}]}$ are the Mn – Mn layers exchange interactions separated by $[\text{Sn}_3]$ and $[\text{Sn}_2\text{Y}]$ layers respectively.